Fracture behavior of natural fiber-reinforced cemented paste backfill under mode-I, mode-II, and mode-III loading: Effect of fiber content and fiber length

By

Michael Hartford

A thesis submitted to the Faculty of Graduate Studies in partial fulfillment of the requirements for the Degree of Master of Science in Civil Engineering

Supervisor: **Dr. Liang Cui**

Associate Professor – Dept. of Civil Engineering

Lakehead University Thunder Bay, Ontario August 2024

Author's Declaration Page

I hereby declare that I am the sole author of this thesis. This is a true copy of the thesis, including any required final revisions, as accepted by my examiners. I understand that my thesis may be made electronically available to the public.

Abstract

The mechanical stability of mine backfill materials is crucial for the safety of mining personnel and production efficiency. When placed into mined-out voids, known as stopes, mine backfill materials are required to provide reliable secondary ground support, which is subjected to finite deformation loading, especially in deep mines. However, due to the quasi-brittle characteristics of cemented paste backfill (CPB), these materials possess very limited post-peak resistance. Enhancing the post-peak engineering performance of CPB is achievable through natural fiber reinforcement techniques. In this study, hemp fibers were selected for their abundant availability in Canada. To investigate their effectiveness in terms of fiber reinforcement, four different fiber lengths (5mm, 10mm, 20mm, and 30mm) and four fiber contents (0.25wt%, 0.5wt%, 1wt%, and 1.5wt%) were employed to prepare the natural fiber-reinforced CPB (NFR-CPB). A series of mechanical tests, including semicircular bend (SCB) tests and end-notched disc bend (ENDB) tests, along with scanning electron microscope (SEM) observations, were conducted on NFR-CPB and control CPB (without fiber reinforcement) at 7 days, 28 days, and 90 days. The results revealed that hemp fiber reinforcement can influence pre-peak behavior and effectively enhance post-peak resistance. Additionally, the results showed that increasing the hemp fiber content and length improved the fracture energy, ductility, and fracture toughness of NFR-CPB. Therefore, the proposed hemp fiber reinforcement approach can be considered a promising method for CPB technology in deep mining applications.

Acknowledgments

I am profoundly grateful to Dr. Liang Cui, my graduate research supervisor, for his confidence in my abilities and encouragement to broaden my knowledge, which led me to undertake this research project. His exceptional leadership and guidance have been vital throughout this journey. Dr. Cui's dedication to civil engineering, laboratory research, and technical writing has significantly influenced my academic growth.

I am also deeply thankful to my thesis committee members, Dr. Jian Deng and Dr. Baoqiang Liao, for their valuable feedback, insightful comments, and encouragement throughout the development of this research. Their expertise and dedication have greatly contributed to the successful completion of this thesis.

Table of Contents:

List of Table and Figures:

Tables

Figures

List of Equations:

Abbreviations:

σ	Normal stress (kPa)
τ	Shear stress (kPa)
φ	Internal angle of friction (°)
ε	Strain (mm/mm)
k_m	Material stiffness (N/mm)
P	Maximum Force (N)
F_p	peak value force (N)
D	Diameter of the sample (m)
t	Thickness of sample (m)
B	Thickness of sample (m)
S	Distance between load frame support bars (m)
W	Width of the sample (m)
a	Notch length (m)
K_I	Mode-I Fracture Toughness ($kPa \cdot m^{1/2}$)
K_{II}	Mode-II Fracture Toughness ($kPa \cdot m^{1/2}$)
K_{III}	Mode-III Fracture Toughness ($kPa \cdot m^{1/2}$)
Y_I	Normalized stress intensity factor for mode-I

Y_{II} Normalized stress intensity factor for mode-II

Y_{III} Normalized stress intensity factor for mode-III

V Volume of sample (cm^3)

w gravimetric moisture content (%)

E_c Fracture Energy (N/mm)

E Elastic modulus (kPa)

c Cohesion (kPa)

Chapter 1 Introduction

1.1 Background

Cement-based materials, including cemented soil, concrete, and cemented paste backfill (CPB), are widely used in construction and mining. After extracting all the mineral ore from an underground site, CPB fills the resulting voids, known as stopes, providing essential support to the surrounding rock structure (Yilmaz, E., 2017). The remaining stopes must be filled using backfilling once the target mineral has been extracted underground. CPB, a mixture comprising approximately 85% waste mine tailings, up to 7% binder, and water, is extensively used for its numerous advantages (Yilmaz et al., 2011). Firstly, CPB significantly reduces the potential for environmental contamination associated with the surface storage of waste mine tailings (Sánchez et al, 2019). By incorporating tailings into the backfill material, CPB minimizes the size of tailings ponds, thus providing substantial economic benefits. Secondly, CPB uses a considerably lower amount of cement binder than traditional concrete. Traditional concrete typically contains around 20% binder, whereas CPB uses only 3-7% (Benzaazoua et al., 2017). This reduction in binder usage is economically advantageous, as the binder is one of the most expensive components in mining operations. Finally, CPB offers superior stability benefits over other backfill methods. Unlike loosely placed rock backfill, which relies on containment by surrounding rock walls, CPB forms a cohesive mass that enhances the structural integrity of the stope. As CPB must support the surrounding rock mass (Cui & Fall, 2016; Ghirian et al., 2016), it is commonly subjected to compressive loading. Once cured, it experiences complex loading conditions due to the surrounding masses and forces induced by ongoing mining operations, such as equipment usage and blasting.

The brittle nature of CPB poses significant challenges for its application. This inherent brittleness, coupled with the complex loading conditions, significantly increases the risk of catastrophic failure. Therefore, it is crucial to develop methods to enhance the implementation of CPB technology and reduce the likelihood of such failures. One promising approach is incorporating fiber reinforcement, improving the material's performance and stability under these demanding conditions. Figure 1.1 shows the placement of CPB and the loading that is placed on the backfill material once poured into the underground stope.

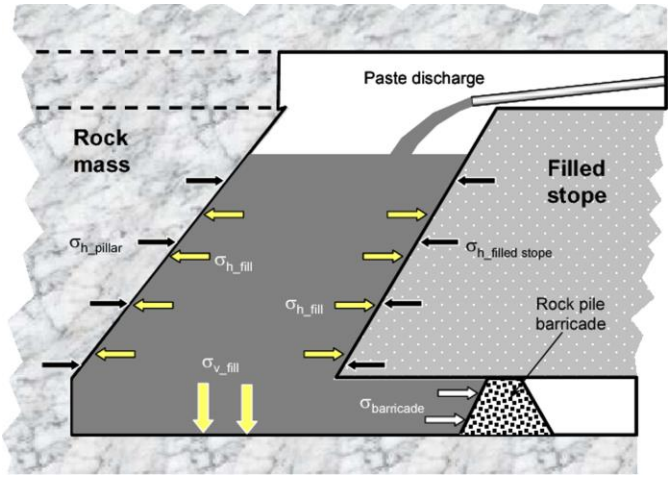

Figure 1.1. Loading conditions present in underground mining (Tikou et al, 2004).

Fiber-reinforced CPB (FR-CPB) is an improvement to conventional CPB. As the strain energy is released from the CPB due to external loading, there is a complete release along fracture planes within the body of the CPB. Once the interparticle matrix has broken, the mechanical performance of CPB mass relies on the post-peak resistance. However, the brittle response of CPB materials may cause catastrophic failure under in-situ loading conditions due to its weak post-peak resistance. Adding fibers into the CPB matrix can effectively prevent crack growth through their bridging effect, forming reliable post-peak

resistance to external loadings. This method can also improve the ductility of the CPB body, enabling the backfill structure to accommodate finite deformation from the surrounding rock mass. Thus, the risk of catastrophic failure is significantly reduced, and the potential for improved ground monitoring of the CPB within the stope is increased.

1.2 Problem statement

Previous research has primarily concentrated on conventional geomechanical behaviors, such as the compressive, tensile, and shear properties of CPB materials (Nasir et al., 2008). Pan et al. (2021) found that higher binder content significantly enhances cohesion and shear strength due to improved cementation. Increasing cement content in CPB leads to higher stiffness and peak load but reduces displacement at peak load, indicating a decrease in ductility (Yunpeng et al., 2024). While these materials are crucial for structural support, they are prone to brittle failure, leading to sudden and catastrophic collapses (Jafari et al., 2021). To address this vulnerability and improve stability in underground mining, incorporating fiber reinforcement into CPB presents a promising approach to reduce the risk of catastrophic failure. The fracture resistance of CPB, encompassing tensile and shear properties, is critical for the stability of CPB structures. Specifically, mode-I, mode-II, and mode-III fracture resistances play vital roles in ensuring the reliability of CPB masses under varying field conditions. Mode-I resistance is crucial for preventing crack propagation within the paste, especially in roof and wall areas where tensile stresses are significant due to overburden pressure and excavation activities (Fang et al., 2023). Mode-II resistance is important along the stope walls to prevent sliding or shearing failures caused by rock layer movement, geological faults, or stress redistribution after ore extraction (Lou et al., 2021). Additionally, mode-III resistance is

essential at the rock-CPB interface, where torsional stresses or twisting forces can compromise the integrity of CPB structures, particularly in areas with uneven ground settlement or seismic activity (Xiu et al., 2023). The complex, multi-directional loading conditions in underground mining often result in the simultaneous development of tensile and shear cracks within the CPB mass (Xiu et al., 2021). Therefore, to facilitate the successful implementation of fiber reinforcement techniques in mine backfill operations, it is of theoretical and practical importance to systematically investigate the fracture behavior and properties of FR-CPB under tensile and shear loading conditions.

Apart from the mechanical performance of the backfill structure, economic performance is another key design criterion of CPB technology. In this regard, natural fibers are preferable to synthetic fibers due to their low environmental impact and economic benefits. According to Khalid et al. (2021), natural fiber-reinforced polymer composites (NFRPCs) offer eco-friendly, lightweight, biodegradable, and cost-effective solutions, making them highly attractive for engineering applications. Väisänen et al. (2017) further support this by highlighting that natural fibers in polymers significantly offset the use of fossil fuels and reduce greenhouse gas emissions, making them a sustainable choice for improving the properties of composites. For example, hemp fiber, known for its high tensile strength, availability, and environmental benefits, offers a sustainable alternative to synthetic fibers (Elfordy et al., 2008; Li et al., 2006). Therefore, a systematic investigation into the fracture behavior and properties of natural fiber-reinforced CPB (NFR-CPB) under mode-I, mode-II, and mode-III conditions is crucial. No studies have been systematically designed to explore the impact of hemp fiber content and length on the fracture behavior of CPB,

highlighting a significant gap in the research. Addressing this gap can contribute to more sustainable and economically viable mining operations.

1.3 Research methodologies

This study employed extensive laboratory experiments to systematically investigate the effects of hemp fiber content and length on fracture behavior and properties of NFR-CPB. The methodologies utilized to achieve this goal are outlined below:

1. Conduct a comprehensive literature review to understand the current knowledge on the mechanical behavior and material properties of cement-based materials influenced by fiber reinforcement. Identify research gaps in the existing body of knowledge, particularly related to the mechanical behavior and properties of FR-CPB.
2. Utilize semicircular bend (SCB) and end-notch disk bend (ENDB) tests to study the fracture behavior of CPB and NFR-CPB specimens. Conduct tests at various hemp fiber contents (0.25%, 0.5%, 1.0%, and 1.5%), lengths (5mm, 10mm, 20mm, and 30mm), and curing times (7 days, 28 days, and 90 days) to reveal the effectiveness of natural fiber reinforcement technique on the fracture response of CPB under tensile and shear loading conditions.
3. Analyze the fracture behavior data to assess the impact of hemp fiber content and length on fracture toughness, stiffness, and fracture energy.
4. Perform scanning electron microscope (SEM) analysis on the microstructure of NFR-CPB specimens. Observe the formation of hydration products within the bulk matrix and fiber-matrix interfacial transition zone. Correlate microstructural changes with variations in mechanical behavior and material properties, facilitating

the identification of mechanisms for the fiber reinforcement effect on the fracture behavior and properties of CPB materials.

1.4 Thesis organization

The research presented in this study is organized into five chapters. Chapter 1 introduces the fundamental information regarding CPB and FR-CPB technology, the problem statement, research methodologies, and overall thesis organization. Chapter 2 summarizes the current state of knowledge from the literature review stage, identifying research gaps and providing the theoretical foundation for the study. Chapter 3 details the preparation of materials and the experimental equipment used in the research, outlining the mechanical testing methods and microstructural observation employed to analyze the material properties of control CPB without fibers and NFR-CPB. Chapter 4 presents a detailed breakdown of the results obtained from the experimental testing program, covering mode-I, mode-II, and mode-III fracture behavior, and discusses the evolution of fracture properties. Finally, Chapter 5 summarizes the findings based on the obtained experimental results, concludes the research work, and provides recommendations for future research to further understand the effects of hemp fiber on NFR-CPB.

Chapter 2 Literature Review

2.1 Introduction

Fiber reinforcement is introduced to enhance the mechanical properties of cement-based materials. Mitchell and Stone (1987) pioneered fiber reinforcement techniques in mine backfill design to optimize cement usage and reduce costs. By increasing the tensile strength and ductility of the backfill, they achieved the desired structural performance with lower cement content. Including fibers helps bridge cracks, distribute stresses more evenly, and improve the material's resistance to deformation and failure, mitigating catastrophic failure risks. The mechanical behavior and properties of FR-CPB have been extensively investigated. For example, Zhao et al. (2023) demonstrated that FR-CPB specimens exhibited higher flexural strength, toughness, and post-peak deflection, primarily due to the fiber bridging effect inhibiting crack expansion. Guowei et al. (2016) utilized polypropylene (PP) FR-CPB samples to reduce brittleness, increase peak compressive strength, and prevent crack propagation and elongation within the samples. This approach significantly enhanced the backfill material's overall mechanical performance and durability.

Fiber reinforcement significantly impacts the mechanical behavior of cement-based materials. Incorporating fibers enhances compressive, tensile, and shear behavior and the elastic modulus and strength. For instance, synthetic fibers such as PP enhance CPB specimens' tensile strength and ductility primarily due to their ability to bridge cracks and distribute stresses more effectively throughout the material (Chen et al., 2019). This results in higher unconfined compressive strength (UCS), improved fracture toughness,

energy dissipation, and post-peak resistance (Jin et al., 2022). The interaction at the fiber-CPB matrix interface, strengthened by cement hydration and matric suction, also improves elastic modulus and hardening behavior over time (Libos et al., 2020). Festugato et al. (2013) comprehensively analyzed the mechanical response of FR-CPB under cyclic shearing. Their findings demonstrated that adding fibers significantly improved the stiffness and hardness of the cemented material. The fibers acted as a reinforcement mechanism, evenly distributing stress throughout the matrix and reducing deformation during cyclic loading. Furthermore, Libos et al. (2021) investigated the impact of curing temperature on PP FR-CPB's time-dependent shear behavior and properties. The results indicated that higher curing temperatures enhance strain-hardening and softening behaviors at early ages, while pre-peak strain hardening becomes less noticeable at advanced ages. This study highlights the importance of considering thermal factors in designing and applying FR-CPB in underground mining operations, suggesting that warmer curing temperatures can improve the material's mechanical properties and durability. Additionally, Park (2011) observed that adding PP fibers to cemented sand significantly enhanced the material's reinforcing effect, with the improvement becoming more pronounced as the fiber content increased. Furthermore, Hou et al. (2024) demonstrated that incorporating fibers (polypropylene, basalt, and rice straw) into CPB enhances its workability, strength, and microstructure while reducing costs. Including fibers significantly reduces bleeding rates and setting times, with PP fiber showing the most notable improvements. Simões et al. (2017) investigated the effects of adding PP, glass, and steel fibers to fiber-reinforced concrete matrices (FRCM). It was found that increasing the fiber content generally enhances compressive strength, with steel fibers

showing the most significant improvement. The addition of fibers also influences bending behavior, cracking loads, and ductility, with steel and PP fibers providing greater ductility and energy absorption capacity than glass fibers, which exhibit more brittle behavior.

To ensure the effectiveness of the fiber reinforcement technique on cemented paste backfill, it is crucial to understand the effects of fiber reinforcement on their mechanical behavior and properties. Therefore, this literature review aims to summarize the effects of fiber parameters, including fiber types, fiber length, and fiber content, on the mechanical response and properties of cement-based materials. This review aims to provide valuable reference information for the engineering design and application of FR-CPB.

2.2 Effect of steel fibers on mechanical behaviors and properties of cement-based materials

Steel fibers are commonly incorporated into cement-based materials to prevent brittle failure and promote higher strain capacity (Prado et al., 2022). They offer excellent resistance to cracking, enhance energy absorption, and significantly improve the material's load-bearing capacity. Steel fibers are particularly effective in reinforcing materials subjected to high tensile and shear stresses. Steel fibers significantly enhance cement-based materials' compressive, tensile, and shear properties. Studies have shown that including steel fibers increases compressive strength, reduces brittleness, and enhances ductility. Steel fibers enhance shear strength and toughness in shear tests, making the material more resistant to deformation and failure (Pakravana et al., 2017). Incorporating strong and rigid fibers in mixed fiber reinforcements significantly enhances cement-based materials' strength, while including low-modulus fibers improves their

ductility and toughness (Figure 2.1). Regarding stress-strain behavior, Abbas et al. (2014) found that steel fiber-reinforced materials exhibit higher peak stress and greater strain capacity than non-rigid materials. Additionally, the bending resistance of concrete reinforced with short steel fibers is superior to that of concrete reinforced with long steel fibers (Figure 2.2).

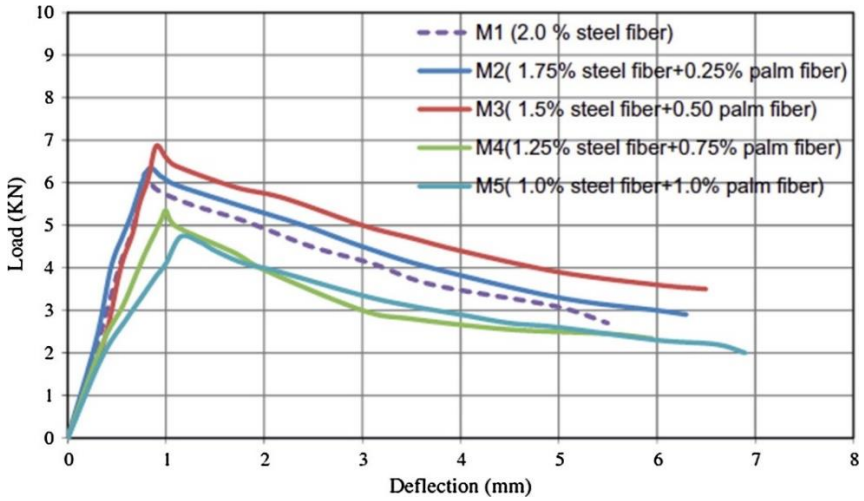

Figure 2.1. Load-deflection curves for high-strength flowing concrete reinforced with hybrid Steel/Palm Fibers (Pakravana et al., 2017).

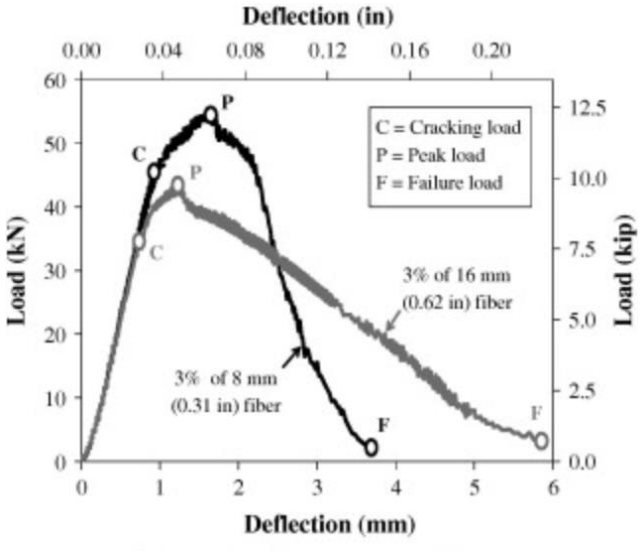

Figure 2.2. Typical load-deflection curve for 3% steel fiber content (Abbas et al. 2014).

Factors such as fiber content and fiber length are crucial in determining the extent of these improvements. Ponikiewski et al. (2014) used X-ray computed tomography to analyze the distribution and spacing of air voids in beams with different volumes of two types of crimped steel fibers. The findings reveal that fibers affect the air void distribution, with notable differences between fiber types and content levels. Wu et al. (2016) examined the effects of straight, corrugated, and hooked-end steel fibers on the mechanical properties of ultra-high-performance concrete (UHPC). Results showed that increased fiber content and the use of deformed fibers reduced flowability but significantly enhanced compressive and flexural strengths. Dupont et al. (2005) presented a method to predict the total number of steel fibers crossing a rectangular section, focusing primarily on calculating an orientation factor. This factor is defined as the average length of the projection of all fibers on the longitudinal axis divided by the fiber length.

Steel fibers significantly influence the mechanical properties of cement-based materials. The elastic modulus, compressive strength, tensile strength, shear strength, and energy dissipation capacity are all improved by adding steel fibers. For example, including steel fibers in high-strength concrete (HSC) reduces the formation of isolated major cracks, resulting in more uniform and controlled cracking under axial compression (Xie et al., 2015). Additionally, the elastic modulus of concrete increases with the addition of steel fibers (Zhang et al., 2021). For instance, the elastic modulus of concrete grades CF40, CF50, and CF60 shows a clear upward trend with increasing steel fiber volume fractions (Figure 2.3).

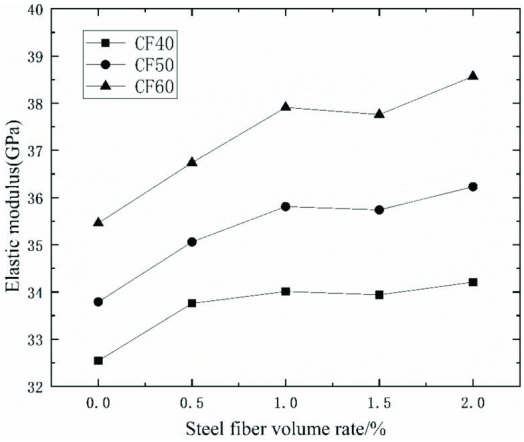

Figure 2.3. The correlation between the elastic modulus of concrete and the content of steel fibers under various concrete grades (Zhang et al., 2021).

Including fiber reinforcement significantly enhances the flexural tensile strength of UHPC due to the fibers' ability to inhibit crack propagation and enhance the ductility of the concrete matrix (Sanya et al., 2023). Furthermore, HSC energy dissipation trends show that specimens with steel fibers have significantly higher energy dissipation than those with PP fiber or plain concrete (Guo et al., 2020). As the volume fraction of PP fiber increases, energy dissipation decreases (Figure 2.4). These findings suggest that incorporating steel fibers substantially enhances the dynamic splitting tensile toughness of HSC, while PP fibers alone are less effective. Generally, flexural tensile strength increases with higher fiber content. However, the tensile strength may decrease at high fiber concentrations due to fiber agglomeration and entrapped air, which can negatively affect the concrete matrix (Larsen et al., 2020).

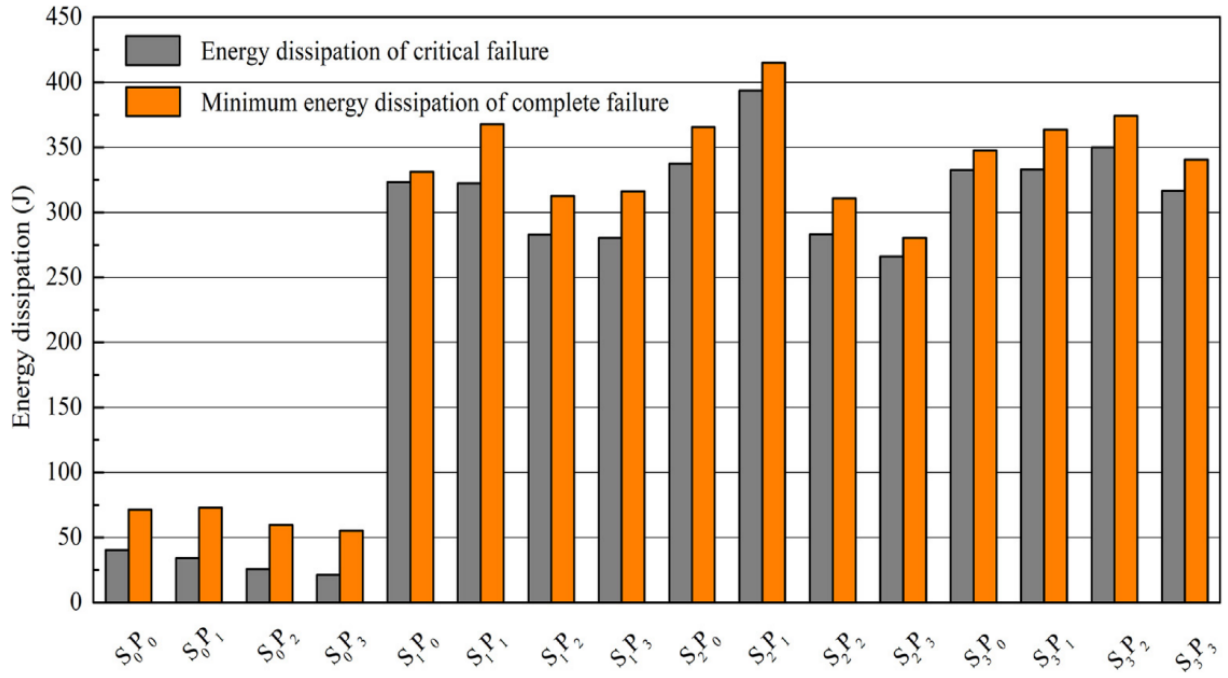

Figure 2.4. The energy dissipation characteristics of high-strength concrete (HSC) under dynamic splitting tension vary with different fractions of steel and PP fibers (Guo et al., 2020).

2.3 Effect of synthetic fibers on mechanical behaviors and properties of cement-based materials

Due to their advantageous properties, synthetic fibers, such as PP, nylon, and polyethylene, are extensively used in cement-based materials. These fibers enhance tensile strength, reducing cracking and improving the load-bearing capacity of cementitious composites (Bentur et al., 2007). They also provide long-term durability and resistance to environmental factors (Hannant, 1978). Additionally, synthetic fibers resist chemical attacks, maintaining integrity in harsh conditions (Banthia & Gupta, 2006). Their low density contributes to the composite materials' overall weight reduction, and they are often more economical than traditional reinforcement methods. These properties make

synthetic fibers valuable additions to cement-based materials, significantly improving their mechanical performance and longevity.

Synthetic fibers improve cement-based materials' compressive, tensile, and shear behavior. This improvement is due to the fibers' ability to distribute stress more evenly within the concrete matrix and inhibit crack propagation, which leads to better performance under tensile loads (Sun et al., 2024). Studies have demonstrated that including PP fibers improves the material's overall toughness and resistance to dynamic and static loads, enhancing its structural integrity and durability (Latifi et al., 2023). Kumar et al. (2006) found that incorporating polyester fibers significantly enhanced highly compressible clay's UCS. The strength increase ranged from 50-68% for 3 mm fibers to over 100% for 6 mm and 12 mm fibers. The study demonstrated that the fibers effectively improved the mechanical performance of the clay by reinforcing the soil matrix and evenly distributing stress. The study conducted by Zhou et al. (2021) investigated the improvement of mechanical properties in sand-based cemented backfill (SCB) by incorporating glass fibers (GF) of various lengths and ratios. The experimental results demonstrate that adding GF enhances the compressive, tensile, and shear strengths of SCB, with optimal mechanical properties achieved using 6 mm fibers at a 1.0% ratio. Specifically, GF increased the compressive strength by 23.7%, tensile strength by 181.2%, and shear strength by 59.7% compared to SCB without fibers. Zhu et al. (2021) investigated the impact of glass fibers on the mechanical performance of shotcrete material reinforced with doped glass fibers. Experimental results showed significant improvements in tensile and shear strengths, with tensile strength increasing by up to 310% and shear strength by 596% when glass fibers were added. SEM analysis revealed

that the glass fibers intertwined and were tightly enveloped by the shotcrete material, enhancing the overall integrity and mechanical strength. Zhu et al. (2021) also investigated the impact of adding GF to sand-based cemented paste backfill (SCPB) used in coal mining, showing that the fibers significantly enhance the early compressive strength. Although the fibers reduce flowability, they create a reinforcing network, increasing compressive strength by up to 679% at early curing stages. The strength improvement stabilizes as curing progresses, highlighting the fibers' role in early-stage structural integrity. Although fibers can enhance the compactness of the CPB matrix, they can also introduce weak structural surfaces, which may negatively impact the overall strength of the CPB (Chen et al., 2020). As illustrated in Figure 2.5, increasing fiber content length does not necessarily correlate with higher CPB strength. The CPB strength varied with fiber parameters and curing ages. At 3 and 7 days, increasing fiber content decreased UCS, while at 28 days, UCS increased with more fiber. A fiber content of 0.22 vol.% was optimal, and varying fiber length affected fiber number, contact area, and distribution uniformity.

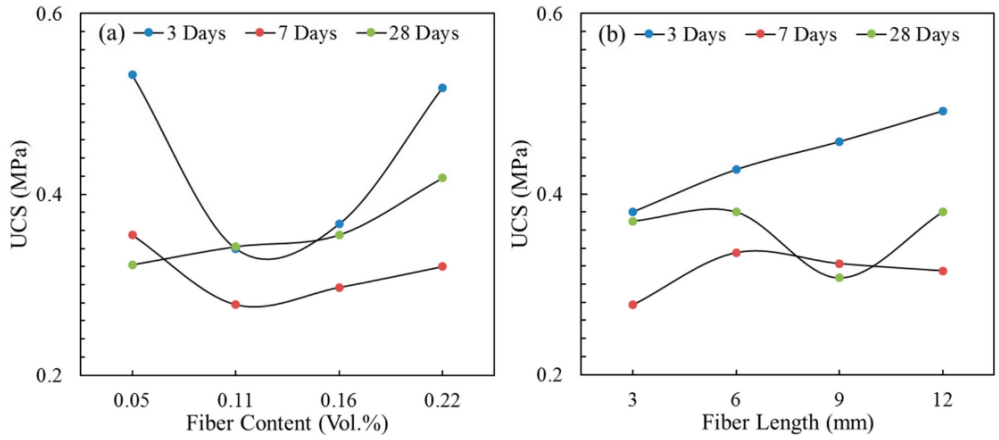

Figure 2.5. The effects of fiber parameters on UCS: (a) fiber content and (b) fiber length (Chen et al., 2020).

Synthetic fibers also enhance cement-based materials' elastic modulus, compressive strength, tensile strength, shear strength, and energy dissipation capacity. Data figures from published works demonstrate these improvements. Jin et al. (2022) found that higher fiber contents and lengths generally result in better mechanical properties and increased energy dissipation during loading. The peak strains of PP FR-CPB samples improved with greater fiber contents within a certain range (Figure 2.6). The specimen without fiber reaches its peak value at a strain of 1.01%. When 0.4% PP fiber is added, the strain of the CPB specimen reaches a peak value of 2.14%. Incorporating fiber into the tailings filling mixture improves the peak compressive strength and transforms brittle failure into ductile failure. The samples exhibited strain-hardening properties as stress increased, indicating that the specimen's strength increased under higher strain due to fiber stretching. Similarly, Balagopal et al. (2022) reported that including synthetic fibers in cementitious composites significantly enhanced their mechanical performance, particularly under dynamic loading conditions. The fibers contributed to improved toughness, ductility, and energy absorption, mitigating the risk of catastrophic failure.

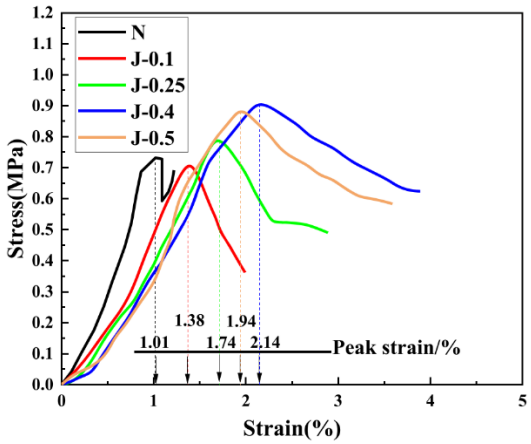

Figure 2.6. Stress-strain curves of three-day curing PP FR-CTB (Jin et al., 2022).

Xue et al. (2019) explored the impact of using PP, polyacrylonitrile, and GF at varying contents. They found that PP fibers provided the highest strength increase (39.6% after 28 days) at an optimal 0.6% content, with similar trends for other fibers. FR-CPB showed improved microstructural integrity and durability, reducing crack propagation. Xue et al. (2020) investigated the effects of fiber length on the strength properties of PP FR-CPB specimens of different sizes. They found that the peak and end strains of cubic specimens were larger than those of cylindrical ones and that specimen size and fiber length influenced the UCS. The optimal fiber length was 12 mm for smaller specimens, while fibers with a length of 18 mm provided the best results for larger specimens. Longer fibers improved the overall structural integrity under load but did not necessarily increase UCS. Yin et al. (2021) investigated the effects of fiber lengths and dosages on cemented sulfur tailings backfill (CSTB). Key findings show that the fluidity of CSTB slurry decreases with added PP fibers, while compressive and tensile strengths peak at 12% sulfur content before declining. Optimal fiber content at 0.6% significantly enhances compressive strength. Fibers were found to reduce late-stage deterioration, with microstructural analysis showing that they enhance load distribution and mechanical properties by creating a spatial skeleton structure. Chen et al. (2023) investigated CPB's mechanical properties and meso-structure characteristics reinforced with multi-size basalt fibers. The research shows that incorporating basalt fibers enhances the compressive and splitting tensile strengths of the CPB, with the optimal fiber blend and size ratio identified (Figure 2.7).

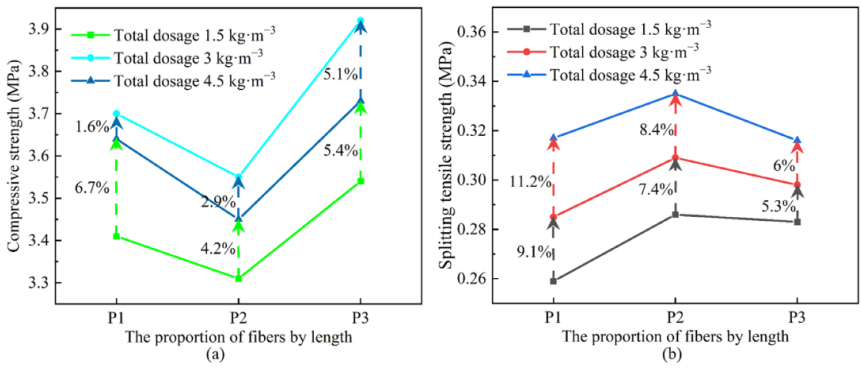

Figure 2.7. The variation in mechanical strength with multi-size basalt fiber (BF) mixing is depicted in terms of (a) compressive strength and (b) splitting tensile strength (Chen et al., 2023).

Wang et al. (2023) explored how basalt fibers affect CPB's mechanical properties, pore structure, and damage characteristics. Adding basalt fibers increases micropores and secondary pores while reducing macropores, which are significantly influenced by fiber content. Basalt fibers enhance peak stress, strain, ductility, and bearing time, with optimal fiber length and content at 12 mm and 1.5%. Additionally, FR-CPB exhibited slower-spreading cracks than samples without fibers, which can help delay failure.

2.4 Effect of natural fibers on mechanical behaviors and properties of cement-based materials

Natural fibers are gaining attention due to their environmental benefits, cost-effectiveness, and mechanical properties. These fibers are renewable, biodegradable, and can significantly enhance the mechanical properties of cement-based materials. For instance, natural fibers such as hemp, jute, and coir have been shown to improve tensile strength, impact resistance, and ductility in concrete composites, making them a viable alternative to synthetic fibers (Yan et al., 2016). Moreover, the cost-performance ratio of natural fibers is favorable, as they are often less expensive than synthetic fibers and can

be sourced locally, reducing material costs and supporting sustainable construction practices (Rocha et al., 2022). Synthetic FR-CPB has significant limitations, including high cost and environmental impact (Yu et al., 2022). This cost reduction is particularly advantageous in large-scale mining operations with substantial backfill material volume.

Natural fibers enhance the mechanical properties of cement-based materials, including compressive, tensile, and shear behaviors. Previous studies have demonstrated that incorporating natural fibers, such as hemp, significantly improves the tensile strength, ductility, and fracture toughness of these materials (Summerscales et al., 2010). Natural fibers like flax, hemp, and jute are increasingly used as cement composites due to their low density, cost-effectiveness, recyclability, and biodegradability (John et al., 2010). The biodegradability of natural fibers makes them environmentally friendly alternatives to synthetic fibers, which are typically non-biodegradable and petroleum-based (Mohanty et al., 2002). This shift towards natural fiber reinforcements supports sustainable construction practices by reducing the carbon footprint and enhancing the performance of cement-based composites. (Bittner et al., 2022). However, these fibers' high moisture absorption leads to poor interfacial adhesion within the matrix. Natural fibers exhibit varying mechanical properties based on the type of fiber and matrix, processing methods, and treatment (Pickering et al., 2016). Kabir et al. (2011) examined how various fiber surface modification methods, such as alkaline, silane, acetylation, benzoylation, and peroxide treatments, improve the mechanical and thermal properties of composites by enhancing fiber-matrix adhesion. It was found that these treatments are essential to optimize the use of natural fibers in composite materials for better performance and durability. Figure 2.8 demonstrates that natural fiber-reinforced materials exhibit

significantly higher peak stress and greater strain capacity than non-reinforced materials, indicating enhanced mechanical performance. Specifically, part (a) shows the UCS curve of fiber-reinforced, solidified soil, where the residual resistance is notably higher, and part (b) illustrates the tensile stress-strain curve of fiber-reinforced, solidified soil (Qiu et al., 2024).

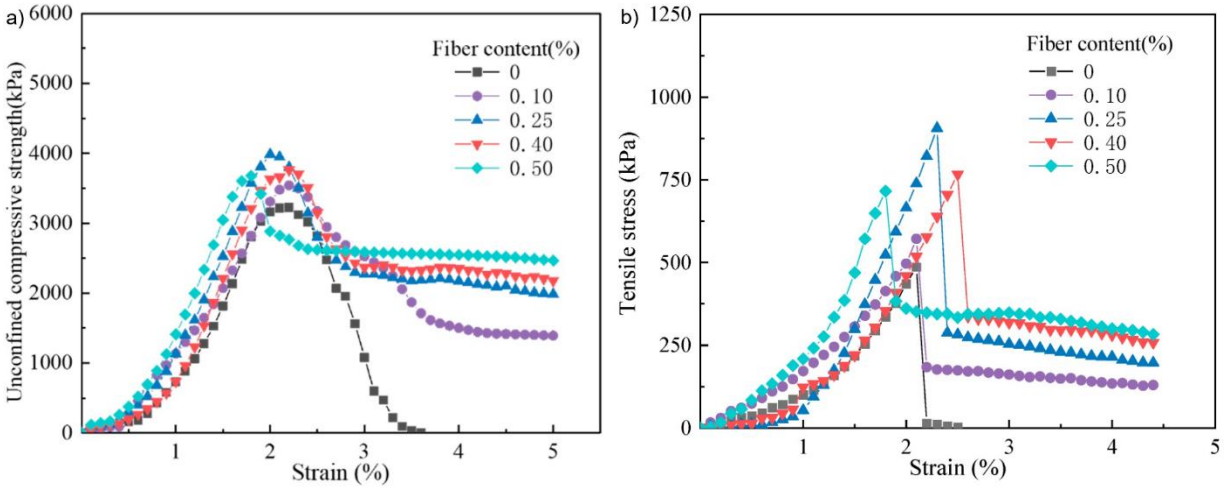

Figure 2.8. (a) Unconfined compressive strength (UCS) curve of fiber-reinforced, solidified soil and (b) Tensile stress-strain curve of fiber-reinforced, solidified soil

Zhou et al. (2017) investigated the engineering properties of hemp fiber-reinforced concrete (HFRC) as a sustainable building material. By pre-treating hemp fibers with a $Ca(OH)_2$ solution, the mechanical properties of concrete, such as tensile and compressive strength, fracture toughness, and ductility, were significantly enhanced. The study found that treated hemp fibers improved the concrete's compressive strength by 10%, tensile strength by 16.9%, and fracture toughness by 7-13% compared to untreated hemp fibers. Additionally, treated fibers increased surface roughness, improving fiber-matrix bonding and resulting in less brittle and more durable concrete composites. Wang et al. (2006) investigated the mechanical and physical properties of HFRC, focusing on

variables like mixing method, fiber content, aggregate size, and fiber length. Results show that compressive and flexural properties of HFRC can be modeled with simple empirical linear expressions, with hemp fiber content being the most significant factor. Çomak et al. (2018) examined the impact of hemp fibers on the properties of cement-based mortars. The study found that adding hemp fibers reduced workability but enhanced mechanical properties, with 2-3% fiber content and 12 mm fiber length yielding optimal results. These optimal conditions improved compressive strength, flexural strength, and splitting tensile strength, while SEM analysis confirmed good adherence of hemp fibers to the cement matrix. Özodabaş (2022) investigated the effects of hemp fibers and shives on the characteristics of cementitious mortars, particularly aiming to enhance ductility and toughness. The experimental results showed that hemp fibers improved the flexural strength of the mortars, whereas hemp shives did not significantly affect flexural strength. Zhou et al. (2016) investigated the impact resistance properties of HFRC. Hemp fibers of 10 mm and 20 mm lengths were incorporated into cementitious composites, and their impact properties were tested at 7, 14, and 28 days using a drop weight impact test. The results revealed that HFRC panels reinforced with 20 mm fibers exhibited higher impact resistance, absorbed more impact energy, and required more impact blows to failure than those with 10 mm fibers. The longer fibers were more effective in inhibiting micro-crack growth and blunting their propagation, thus improving the composite's overall durability and impact resistance. Li et al. (2006) investigated the impact of fiber content and fiber length on HFRC performance. Results showed that fiber content up to 1.06% by weight and fiber lengths of 10-30 mm optimally enhances flexural toughness and impact resistance. However, increasing fiber content reduces compressive strength, indicating

the need to balance these factors for optimal HFRC properties. Additionally, sisal fiber SF reinforcement in cement-based composites significantly enhances fracture toughness, flexural strength, and resistance to various stresses while being cost-effective and environmentally friendly (Toledo et al. 1999). Ahmad et al. (2022) found that incorporating SF improves tensile and flexural strengths, although it reduces the workability and increases water absorption of concrete. Treatments like NaOH-clay enhance the fiber-matrix interaction, improving performance and durability. Despite its benefits, concrete density decreases with higher SF content, and the material exhibits increased water absorption. Veigas et al. (2022) investigated SF as a sustainable alternative to synthetic fibers in cementitious composites. Two coatings, polyester resin, and bio-based shellac, were examined to address the potential degradability of SF. Various mixtures with different dosages of uncoated and coated fibers were tested for compressive, splitting tensile, and flexural strengths. Results showed notable improvements in tensile and flexural strengths, with increases of 20% and 42%, respectively, compared to mixtures without fibers. Weathering tests indicated that uncoated and shellac-coated fibers performed better under wet/dry cycles, maintaining strong bonds with the cementitious matrix and avoiding significant degradation. Additionally, sisal fibers effectively mitigated plastic shrinkage-induced cracks, proving a viable alternative to synthetic fibers for high-performance cementitious composites. Furthermore, (Li et al., 2022) demonstrated that adding rice straw (RS) fibers significantly enhances the tensile strength of CPB, particularly in the early stages of curing. The effects of RS fiber length and content on average peak strains are shown in Figure 2.9. In part (a), the peak strain initially decreases and then increases with rising RS fiber content at 3 and 28 days of curing, indicating an optimal fiber content

that maximizes peak strain. Part (b) shows that peak strain increases with longer fibers, then decreases, suggesting an optimal fiber length for enhanced peak strain at the same curing ages.

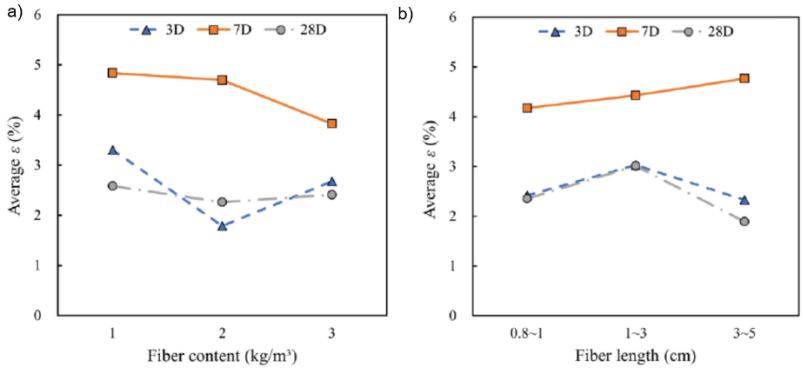

Figure 2.9. The influences of RS fiber on peak strain. (a) Average ε at different RS fiber contents and (b) average ε at different RS fiber lengths (Li et al., 2022).

Chompoorat et al. (2023) examined how incorporating palm fibers into cement-treated sand (CTS) enhances flexural performance and microstructure. The optimal flexural performance was achieved with 1% fiber content and 40 mm fiber length, significantly improving strength and ductility. Buathong et al. (2023) examined how palm fibers enhance CTS's compressive strength and ductility. The findings indicate optimal fiber reinforcement (1% content, 40 mm length) significantly improves peak strength and toughness while reducing brittleness. The findings suggest that palm fiber-reinforced CTS suits pavement structures due to its improved toughness, residual strength, and reduced cracking. Ali et al. (2012) explored the potential of using coconut fibers as reinforcement in concrete structures, especially in tropical earthquake regions. The findings reveal that structures with 5 cm long fibers and 5% fiber content exhibit the greatest mechanical and

dynamic properties, including increased compressive strength and toughness. However, it results in a lower elasticity and density modulus than plain concrete.

Natural fibers also enhance cement-based materials' elastic modulus, compressive strength, tensile strength, shear strength, and energy dissipation capacity. Data figures from published works demonstrate these improvements. The higher fiber content and length generally result in better mechanical properties and increased energy dissipation during loading. A study by Ahmad et al. (2020) investigated the impact of incorporating coconut fibers of different lengths and varying contents on the mechanical properties of high-strength concrete (HSC). The research reveals that adding coconut fibers improves the compressive, splitting tensile, and flexural strengths of HSC. The optimal combination of 50 mm fiber length and 1.5% content by mass yields the best overall results (Figure 2.10), significantly enhancing energy absorption and toughness indices. Additionally, the study employs SEM to analyze the microstructure of the reinforced concrete, showing better bonding and reduced crack propagation due to the fiber addition.

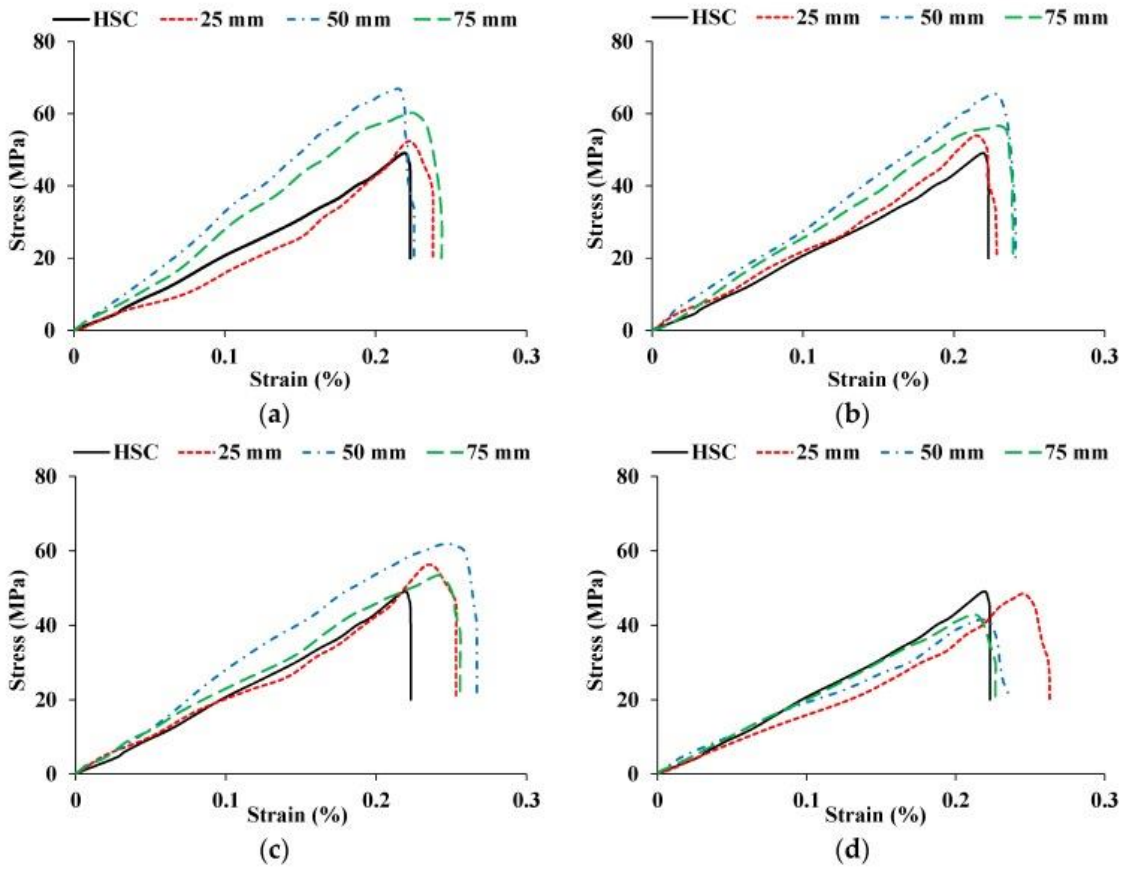

Figure 2.10. Stress-strain curves for HSC and coconut fiber-reinforced HSC with a fiber content of (a) 0.5%, (b) 1%, (c) 1.5%, and (d) 2% (Ahmad et al., 2020).

Furthermore, Ahmad et al. (2023) investigated the potential of bamboo fibers in concrete reinforcement to enhance tensile and flexural capacities while reducing brittle failure. Bamboo fibers improve impact resistance and performance at elevated temperatures but increase water absorption, negatively impacting durability. Optimal fiber content should be between 1-1.5% by weight of the binder for best results. Libre et al. (2023) also investigated the mechanical properties and durability of cement composites reinforced with bamboo fibers. Optimal results were found with 20 mm fibers at 1.4% loading, leading to a 292.41% increase in compressive strength and a 355.82% increase in split tensile strength compared to control samples. SEM analyses confirmed the microstructural

improvements, with significant findings such as forming Si-O-C bonds and better bonding between fibers and the matrix. The study concludes that bamboo fiber-reinforced cement composites can significantly reduce the carbon footprint of construction materials while providing enhanced mechanical properties suitable for plastering and retrofitting applications. Jiao et al. (2016) investigated using natural cellulose nanofibers (CNFs) to enhance the mechanical properties and sustainability of cement composites. The study revealed that adding 0.15% CNFs by weight to cement paste increased flexural and compressive strengths by 15% and 20%, respectively. This improvement is due to a higher degree of hydration and a denser microstructure facilitated by CNFs, which enhance the hydration process, reduce porosity, and improve bonding within the cement matrix. Also, surface chemical modifications and proper dispersion techniques are essential to improve compatibility with polymer matrices and achieve the desired mechanical performance in the resulting nanocomposites (Dufresne, 2017).

2.5 Summary

Fiber reinforcement techniques significantly enhance the mechanical behavior and properties of cement-based materials. Adding synthetic or natural fibers improves the compressive, tensile, and shear strength and the elastic modulus and energy dissipation capacity of these materials. Steel fibers, for instance, are well-known for their high tensile strength and durability, which contribute to the improved structural integrity of concrete. Synthetic fibers, such as polypropylene, offer benefits like reduced plastic shrinkage cracking and increased impact resistance. Natural fibers provide a sustainable alternative, enhancing mechanical properties while promoting environmental sustainability.

Fiber reinforcement holds substantial potential for CPB technology by improving mechanical performance and structural reliability. Natural fibers present a promising option due to their cost-effectiveness and environmental benefits. Hemp fibers, for instance, are abundant, renewable, and biodegradable, making them an attractive choice for sustainable construction practices. Their integration into CPB can potentially improve the mechanical behavior and properties, such as the backfill material's material strength and fracture toughness, addressing economic and environmental concerns.

Despite the recognized benefits of fiber reinforcement, synthetic fibers in CPB have limitations, including higher costs and environmental impacts. This study seeks to overcome these challenges by investigating the use of natural fibers, specifically hemp, to enhance the mechanical properties of CPB. The primary objectives are to examine the effects of varying hemp fiber content and fiber length on CPB's fracture behavior, fracture properties, and microstructure. By exploring these factors, the study aims to fill the existing research gap and provide valuable insights into the practical application of hemp fibers in CPB materials, promoting sustainability and performance improvements.

Chapter 3 Experimental Testing Program

3.1 Materials

Tailings are fine-grained residues that remain after extracting valuable minerals from ore. These residues consist of crushed rock and processing fluids, often containing various minerals and chemicals used during extraction (Blowes et al., 1991). Artificial non-acid-generating tailings, precisely ground silica (manufacturer: US SILICA), were utilized to prepare the NFR-CPB mixture due to their consistent quality (99.5% SiO_2). Ground silica, predominantly composed of quartz, is a significant byproduct extracted from hard rock mines, where the primary focus is often on mining valuable ores such as gold, copper, and nickel. Unlike natural tailings, which often contain sulfide or other reactive minerals (Gou et al., 2019), ground silica tailings' mineral and chemical compositions are closely controlled. This reduction in uncertainties is crucial for the accurate interpretation of experimental results. Figure 3.1 presents a particle size distribution for the ground silica material. This graph illustrates the cumulative volume percentage of particles across a range of sizes, from 0.1 to 1000 micrometers (μm). Table 3.1 shows the grade curve characteristics of the particle size distribution, characterized by the diameters at which certain percentages of the material pass through, specifically D10, D30, and D60. The particle size distribution of this ground silica material indicates a well-graded composition, which enhances its mechanical properties, such as packing density and structural stability. Furthermore, the investigation utilized White Portland Cement Type I (PCI) manufactured by Ash Grove as the binding agent and tap water as the mixing medium for the NFR-CPB specimens. Hemp fibers were selected as the fiber reinforcement of choice for many reasons. Firstly, hemp cultivation is remarkably cost-effective. This is due to its

minimal need for inputs such as pesticides and fertilizers, as hemp is naturally resistant to most pests and diseases (Ahmed et al, 2022). Additionally, hemp proliferates and thrives in a variety of soil conditions, which further reduces the need for intensive agricultural practices and costly soil amendments (Visković et al, 2023). These factors make hemp a significantly cheaper alternative to synthetic fibers, as the production costs are much lower. Its fibers are characterized by their robust tensile strength and durability, making them an excellent reinforcement material in construction (Abdalla et al, 2022). The combination of cost-efficiency, sustainability, and strength positions hemp fiber as an ideal candidate for construction solutions.

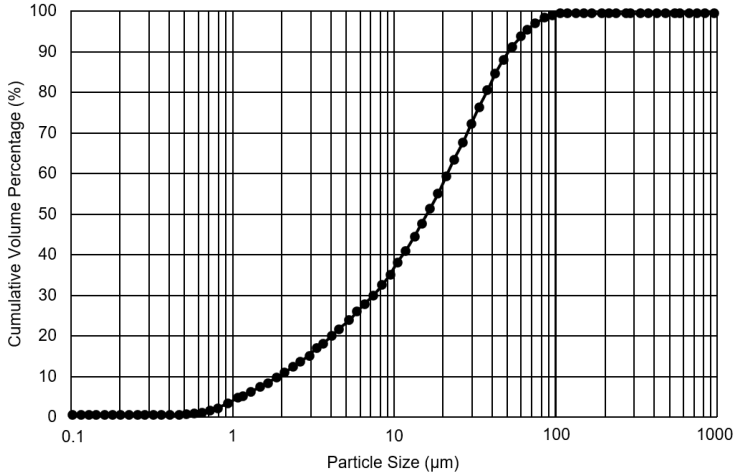

Figure 3.1. Particle Size Distribution.

Table 3.1. Grade Curve Characteristics.

D10 (µm)	D30 (µm)	D60 (µm)	Cu (-)	Cc (-)
2.22	9.52	27.60	12.42	1.48

3.2 Mix proportions and specimen preparation

The CPB paste was prepared with a cement content of 4.5 wt.% (wt.%: weight percentage), and a water-to-tailing ratio of 0.36. Consequently, the resultant paste possesses a solid content of 74.42wt.%. The selection of fiber length and fiber content was based on the typical fiber parameters adopted in previous studies. Table 3.2 shows fiber contents and lengths commonly adopted for reinforcing cement-based materials. Specifically, fiber contents ranging from 0.05 wt% to 1.5 wt% and fiber lengths from 3 mm to 24 mm are typically used across different studies. For instance, Festugato et al. (2017) utilized PP fibers of 6, 12, and 24 mm lengths with a 0.5 wt% content, while Xue et al. (2019) used fibers of 6, 12, and 18 mm lengths with a 0.6 wt% content. Other studies, such as those by Chakilam et al. (2020), Gao et al. (2023), and Chen et al. (2020), have employed various combinations of fiber lengths and contents. Xue et al. (2020) investigated the effects of fiber length on the strength properties of PP FR-CPB specimens of different sizes. They found that the peak and end strains of cubic specimens were larger than those of cylindrical ones and that specimen size and fiber length influenced the UCS. The optimal fiber length was 12 mm for smaller specimens, while fibers with a length of 18 mm provided the best results for larger specimens. Based on this research, this study adopted four specific fiber contents (0.25, 0.5, 0.75, and 1 wt%) and four fiber lengths (5, 10, 20, and 30 mm) to prepare NFR-CPB specimens (Table 3.3). These selected parameters are within the commonly used ranges, ensuring a comprehensive evaluation of hemp fiber's effectiveness in enhancing the mechanical properties of CPB.

A three-phase procedure was utilized to prepare the hemp fibers. First, a paper barrier was used to contain the fibers effectively during the cutting process to cut the hemp fiber to the desired lengths (i.e., 5, 10, 20, and 30mm). This method involves placing the hemp fibers inside a rolled paper barrier and then positioning them under a guillotine paper cutter. The paper barrier helps keep the fibers aligned and contained, ensuring a clean and precise cut. This technique minimizes the loss of fibers and ensures uniformity in fiber length for subsequent processing and treatment. Second, hemp fibers with desired lengths were chemically treated with sodium hydroxide to remove the lignin and hemicellulose. Sodium hydroxide was chosen for its effectiveness in breaking down these components, thus improving the adhesion between the fibers and the cement matrix, which is crucial for enhancing the reinforcing effect of the fibers in cement-based materials (Widodo et al., 2023). After the sodium hydroxide treatment, the hemp fibers were thoroughly washed to remove any remaining impurities and alkaline residues that could interfere with the bonding process. Third, the fibers were oven-dried at 50°C for 24 hours, and the dried fibers were teased and then carded to align and separate the fibers, creating a more uniform and consistent fiber material. The details of this three-phase procedure is illustrated in Figure 3.2. The treated hemp fibers were incorporated into the mixture. The resulting blends were thoroughly mixed using a mixer and then cast into cylindrical molds with a diameter of 100 mm and a height of 200 mm, made from high-density polyethylene (HDPE). Meanwhile, a group of control CPB samples without fibers was also prepared. These samples were cured at room temperature and sealed from air for 7 days, 28 days, and 90 days.

Table 3.2. Fiber length and content commonly adopted in practice

Fiber type	**Fiber length (mm)**	**Fiber content (wt. %)**	**Reference**
Polypropylene	6, 12, 24	0.5	Festugato et al. (2016)
Polypropylene	6, 12, 18	0.6	Xue et al. (2019)
Polypropylene	6, 9, 13	0.25, 0.5, 0.75	Chakilam et al. (2020)
Polypropylene	6, 12	0.3, 0.6, 0.9	Gao et al. (2023)
Polypropylene	3, 6, 9, 12	0.05, 0.11, 0.16, 0.22	Chen et al. (2020)
Glass Fiber	3, 6, 15	0.5, 1, 1.5	Zhou et al. (2021)
Recycled Tire Polymer Fiber	16	0.3, 0.5	Wang et al. (2021)

Table 3.3. Summary of mix recipe of NFR-CPB.

Cement content (wt.%)	Water-to-tailing ratio (-)	Fiber lengths (mm)	Fiber contents (wt.%)	Curing times (days)
4.5	0.36	5, 10, 20, 30	0, 0.5, 1, 1.5	7, 28, 90

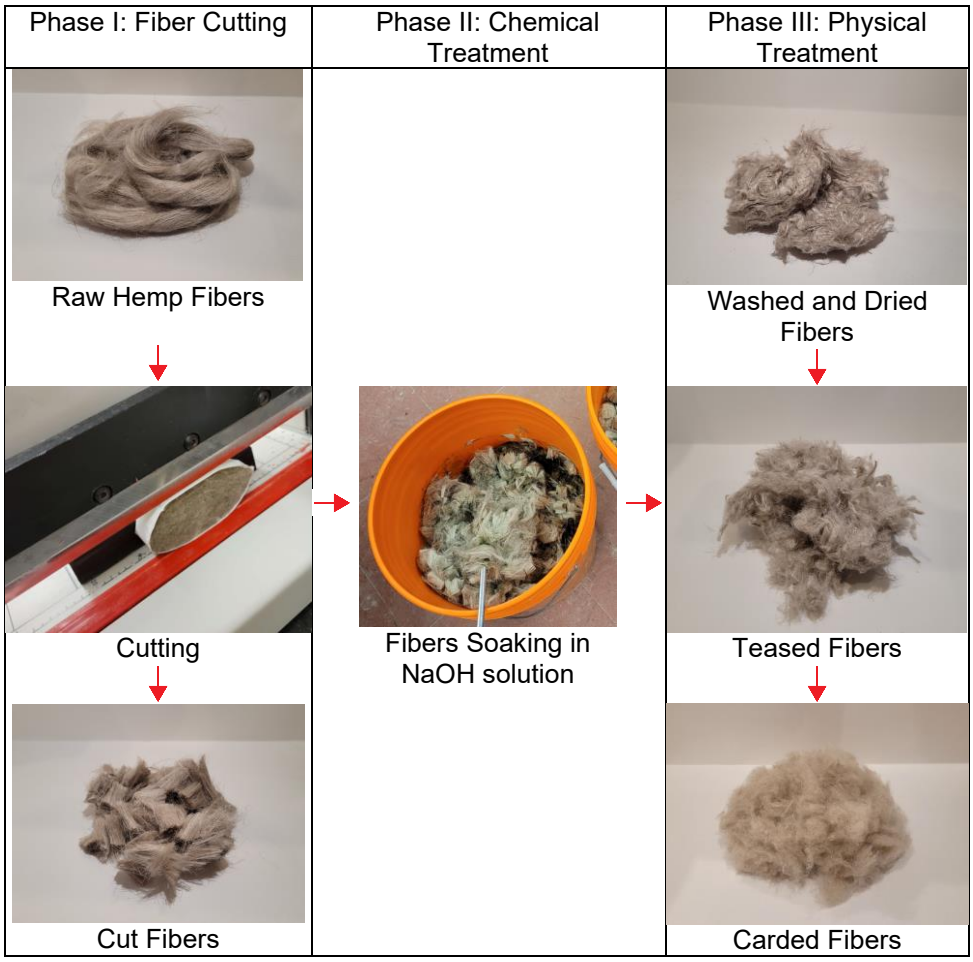

Figure 3.2. Three-phase preparation procedures of natural hemp fibers.

3.3 Semicircular bend (SCB) test

The geometry and loading conditions of cracked specimens significantly influence fracture toughness results, making it crucial to evaluate the differences in measured values for accurately assessing various construction materials (Karimi et al., 2023). The semicircular bend (SCB) test is commonly used worldwide to determine mode-I and mode-II fracture behavior, particularly in rock and brittle materials (Bažant et al., 1983). Its simplicity and convenience make it especially suitable for brittle materials such as concrete (Kuruppu et al., 2012). In this test, three-point bending is applied using a

laboratory compression machine, with load, displacement, and fracture characteristics continuously monitored. Mode-I SCB tests assess the material's response to tensile stresses, whereas mode-II SCB tests examine fracture response under in-plane shear stress (Shi, 2009). Mode-I fracture is most common in areas with little or no confinement, such as the roof or exposed surfaces of the CPB. These areas experience tensile forces from the weight of the surrounding material or external loads, leading to cracks opening. Mode-II fractures are caused by in-plane shear forces that act parallel to the crack. These fractures are particularly prevalent in regions near the boundaries of CPB layers or where the CPB interacts with structural elements like rock walls. The cutting procedure involved multiple steps to achieve the desired SCB samples, as shown in Figure 3.3. First, the CPB samples were de-molded by puncturing the bottom with a nail and using an air compressor to remove the cylindrical specimens. Next, 50mm intervals were carefully marked along the cylinder using a precision ruler. A professional miter saw was then used to make initial cuts, producing disk samples of 100mm diameter and 50mm width, which were then halved to create six semi-circular disk samples. After that, a centerline was marked on each semi-circular disk, followed by the introduction of a 25mm notch. Mode-I SCB specimens featured a 90-degree notch, while mode-II SCB specimens had a 54-degree notch. Finally, each SCB specimen underwent a thorough inspection to verify dimensions and ensure adherence to the defined parameters for SCB tests. For repeatability of results, a minimum of three specimens were tested for each curing condition. Moreover, three control SCB samples without hemp fibers were also prepared. The SCB specimen was positioned on two supporting bars with its notched side oriented downwards during testing. A centrally aligned loading bar was positioned directly above

the specimen's notch and equipped with an S-type load cell (manufacturer: ARTECH Industries Inc.) to record the applied force. A displacement transducer (manufacturer: A-Tech Instruments Ltd.) was placed to measure the displacement. A micro-measurements' System 8000 data acquisition system, interfaced with the load cell and displacement transducer, continuously captured force and displacement data throughout the testing phase. As a result, 306 samples were prepared and tested under mode-I and mode-II SCB tests.

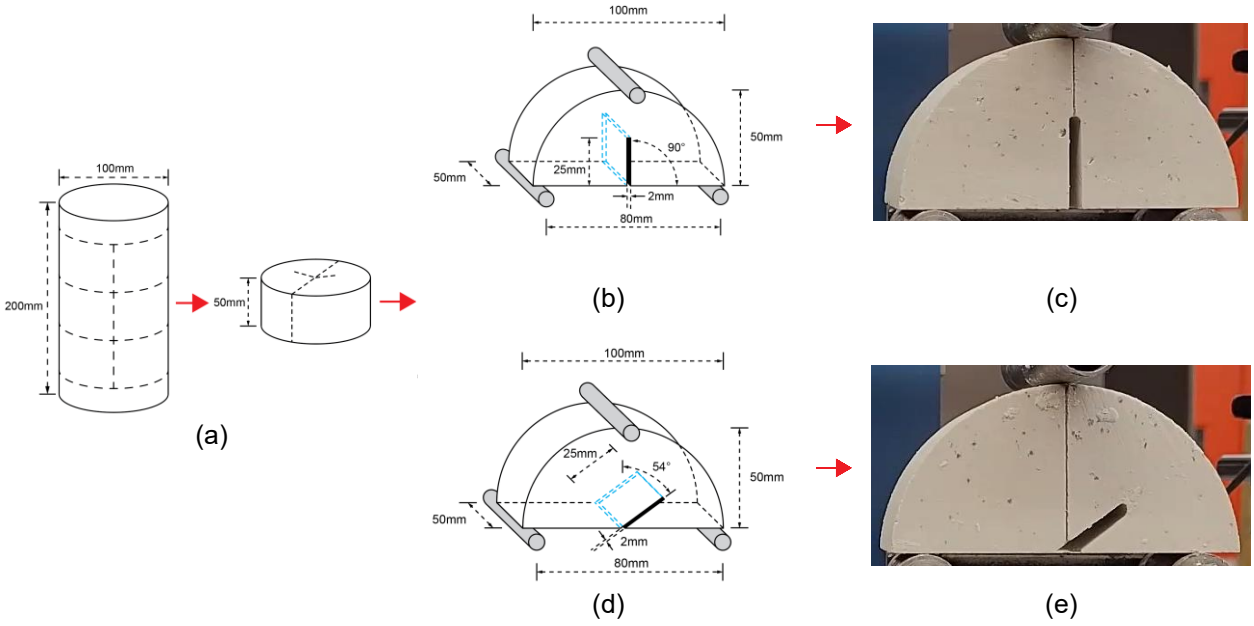

Figure 3.3. Schematics of (a) SCB sample preparation, (b) dimensions of mode-I SCB sample, (c) experimental setup of model-I SCB, (d) dimensions of mode-II SCB sample, and (e) mode-II SCB experimental setup.

3.4 End-notched disk bend (ENDB) test

The mode-III edge notch bending (ENDB) test is used to study the out-of-plane shear behavior of materials, particularly the mode-III fracture properties, as described by Aliha et al. (2015). Mode III fracture behavior differs significantly from mode-I and mode-II

fractures (Suresh et al., 1987). Mode-III fractures arise from out-of-plane shear forces, which cause a twisting or tearing action along the crack front. These fractures will likely occur near the interface between CPB and rock or other structural boundaries. During fracture, the first suitably oriented microcrack initiates sample failure, as numerous microcracks can link up and lead to the cleavage or intergranular fracture of the entire specimen (Liu et al., 2004). The CPB samples were first de-molded to prepare the specimens for testing by puncturing the bottom with a nail and using an air compressor to remove the cylindrical specimens. Next, 50mm intervals were carefully marked along the cylinder using a precision ruler. Before cutting, the miter saw blade was inspected for any signs of wear, damage, or misalignment. The miter saw was then used to make several cuts, producing 100mm diameter and 50mm width disks. Each layer was utilized for one mode-III test, with approximately 25mm of surplus material removed from both ends of each specimen. A centerline was marked on each disk; then, a 20mm notch was introduced perpendicularly through the specimen (Figure 3.4). A total of 153 samples were tested under ENDB tests. The ENDB tests were conducted via the testing machine and a data logging system like the SCB tests. To ensure the repeatability of test results, a minimum of three ENDB specimens were tested.

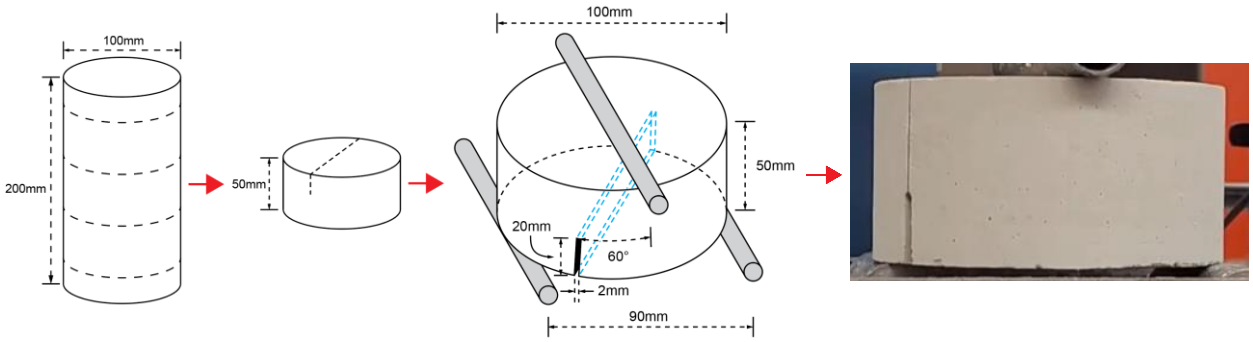

Figure 3.4. Schematics of (a) ENDB sample preparation, (b) dimensions of ENDB sample, and (c) experimental setup of ENDB test.

3.5 Determination of fracture properties of NFR-CPB

Based on the measured load-displacement curves from SCB and ENDB tests, a series of fracture properties, including material stiffness, fracture toughness, and fracture energy, can be extracted. These properties are critical for understanding the influence of hemp fibers on the fracture behavior of CPB materials. While a strength-based design method is commonly employed, its primary limitation is that it only considers the peak load and does not account for the energy required for crack initiation and propagation. This limitation emphasizes the need to study fracture energy and toughness, which provide a more comprehensive assessment of a material's behavior under stress, particularly for materials like CPB, where energy absorption is a key performance factor. As shown in Figure 3.5a, the most consistent slope for stiffness was determined using values between 40% and 60% of the peak load:

$$k_m = \frac{60\%F_p - 40\%F_p}{D_{60} - D_{40}} \quad (3.1)$$

where k_m is the material stiffness (N/mm), F_p is the peak value force, D_{60} is the displacement corresponding to 60% peak load (mm), and D_{40} is the displacement corresponding to 40% peak load (mm).

Secondly, fracture toughness offers critical insights into a material's ability to resist crack propagation under stress (Sharma et al., 2021). In contrast to the strength-based method, fracture toughness values—denoted as K_I, K_{II}, and K_{III} for mode-I, mode-II, and mode-III loading, respectively—measure the material's resistance to sudden fracture. These values are especially important when considering the brittle nature of CPB materials, as they ensure the material can withstand stress without catastrophic failure. The fracture toughness values under SCB and ENDB tests were calculated as follows:

$$K_I = \frac{P}{DT}\sqrt{\pi a}Y_I \tag{3.2}$$

$$K_{II} = \frac{P}{DT}\sqrt{\pi a}Y_{II} \tag{3.3}$$

$$K_{III} = \frac{6PS}{RB^2}\sqrt{\pi a}Y_{III} \tag{3.4}$$

where P is the maximum force (N), D is the diameter of the semicircular specimen (mm), T is the thickness of the semicircular specimen (mm), a is the notch length (mm), and Y represents the normalized stress intensity factor (with values Y_I = 6.52, Y_{II} = 1.072, and Y_{III} = 0.0713).

The diameter and thickness of the specimen directly affect stress intensity and distribution. Larger diameters and thicknesses increase load-bearing capacity, while the notch length and orientation influence stress concentration and fracture mode (I, II, or III).

Lastly, fracture energy is required to initiate and propagate a crack until total material failure (Lee et al., 2014). Unlike strength-based design, which focuses solely on peak load, fracture energy accounts for the area under the load-displacement curve and is essential for understanding how materials behave over the fracture process. Fracture energy is calculated as the area under the load-displacement curve (Figure 3.5b). This is especially relevant for composite materials like NFR-CPB, where energy absorption is key in performance. Fracture energy is calculated using the following equation:

$$E_c = \sum_{i=1}^{n-1} \frac{(F_i + F_{i+1})}{2(D_i - D_{i+1})} \tag{3.5}$$

where E_c (N/mm) is the cumulative stiffness of the material. F is the force applied, where F_i and F_{i+1} are the peak values of force at consecutive measurement points i and $i+1$, respectively. D denotes the displacement, where D_i and D_{i+1} represent the displacement corresponding to 60% of the peak load at measurement points i and $i+1$, respectively.

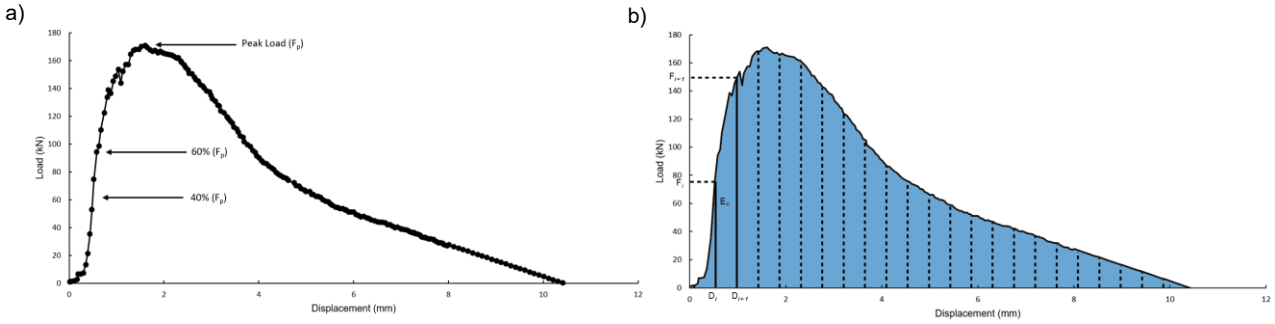

Figure 3.5. Definition of fracture properties of CPB: a) material stiffness (k_m) and b) fracture energy (E_c).

These three properties—material stiffness, fracture toughness, and fracture energy—are important for evaluating the performance of NFR-CPB, as they provide a comprehensive view of the material's behavior beyond what peak load measurements can offer. Understanding these properties is essential to improving the design and durability of CPB materials reinforced with natural fibers like hemp.

3.6 Scanning electron microscope (SEM) analysis

As a type of composite material, the fracture response of NFR-CPB is governed by its microstructure. SEM analysis offered insight into the influence of hemp fiber on the matrix structure. To achieve such results, the equipment utilized was a Hitachi SU-70, which scanned a focused electron beam over the sample's surface, generating various signals that were transformed into image data. A multi-step preparation process was followed before the SEM analysis of the NFR-CPB specimen. It started with sanding a slide to achieve a smooth, even surface, free from any irregularities or contaminants that could interfere with the microscopic examination. Once the slide was prepared, a tiny flake of the NFR-CPB sample was adhesively secured onto it, ensuring it stayed firmly in place during the analysis. The slide with the adhered hemp flake was coated with a thin gold layer to enhance the sample's conductivity and the quality of electron imaging in the SEM. This helped mitigate charging effects that might distort the SEM images and enhanced surface topographical contrasts for more detailed visualization. With the sample primed, the SEM was used to analyze the surface, revealing the NFR-CPB's intricate structural and morphological details and providing valuable insights into its microstructural characteristics. Control samples with no fiber and 20mm hemp fibers at a 1% concentration were analyzed for the SEM analysis. The samples were examined at 7, 28, and 90-day curing times.

Chapter 4 Experimental Results

4.1 Load-displacement curves of NFR-CPB

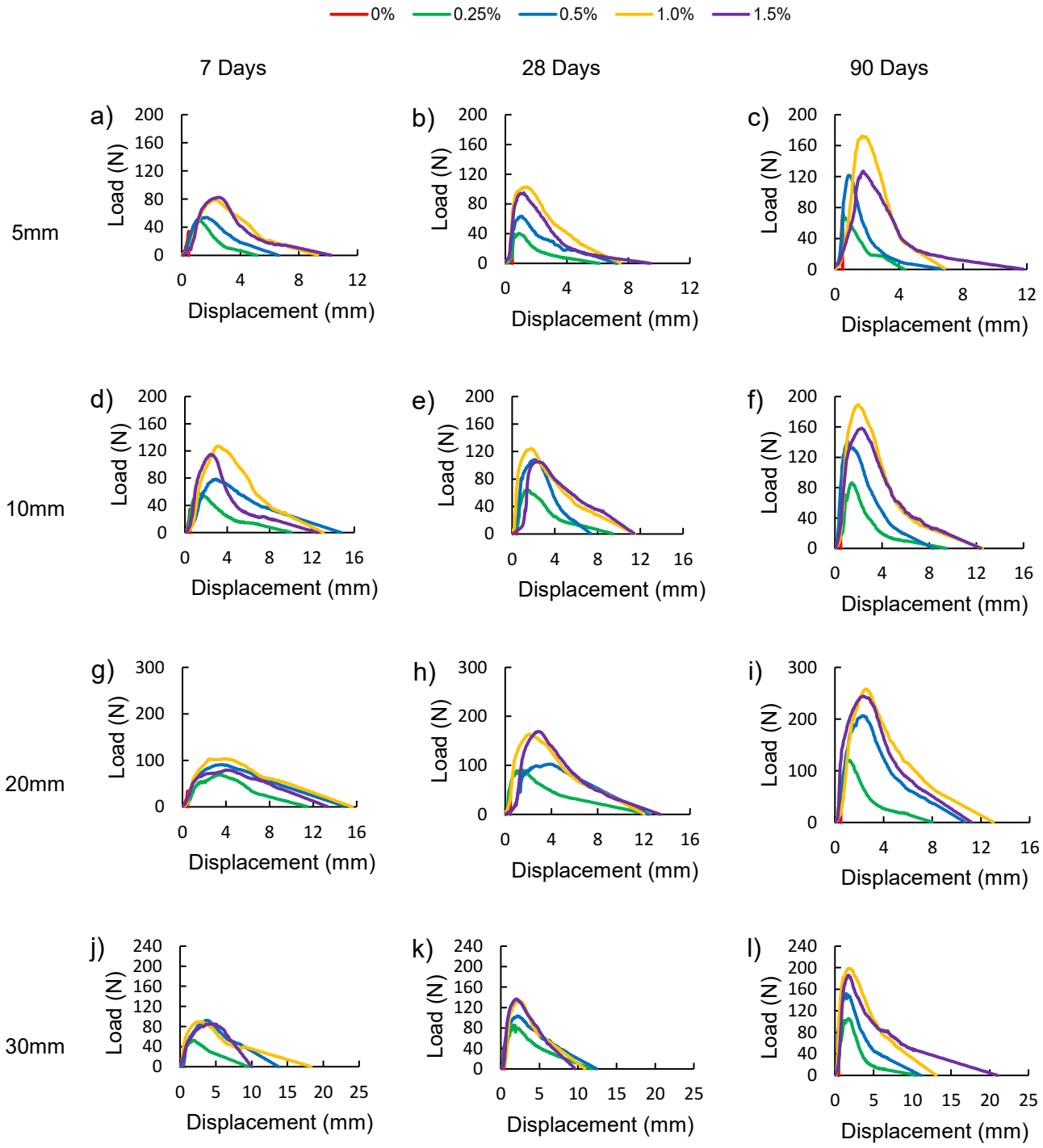

Figure 4.1. Mode-I load-displacement curves of NFR-CPB at different curing times.

The mode-I load-displacement curves of NFR-CPB at different curing times are illustrated in Figure 4.1. It can be observed that compared with control CPB without natural fiber reinforcement, the inclusion of hemp fibers can influence both pre- and post-peak behavior of CPB under mode-I loading conditions. For the pre-peak behavior, adding hemp fibers causes the deviation of pre-peak branches from the counterparts measured from control CPB. Moreover, natural fiber reinforcement consistently increases the peak resistance load. The extent of peak resistance load reinforcement is sensitive to fiber content and fiber length. For instance, CPB with 5mm fibers exhibited a lower peak load with a rapid post-peak decline, likely due to insufficient fiber length to bridge cracks effectively. CPB with 10mm fibers showed a moderate peak load and similarly brittle post-peak response. In contrast, the 20mm fiber achieved the highest peak load with a more ductile post-peak behavior, demonstrating its effectiveness in enhancing toughness and bridging cracks. The 30mm fiber exhibited a similar peak load to the 20mm fiber but with a more gradual post-peak decline, indicating sustained load transfer even after peak load. For the post-peak response, tolerance to the displacement can be significantly increased as the fiber length increases. However, when the fiber length exceeds 20mm, a weakened tolerance to displacement appears at an advanced age. The obtained results demonstrate the effectiveness of hemp fiber reinforcement on the mechanical behavior of CPB. Besides the influence of fiber length and fiber content, hemp fiber reinforcement is also governed by the curing time, i.e., the progression of binder hydration in the tailing matrix. NFR-CPB features a higher peak resistance and a weakened tolerance to deformation at advanced ages.

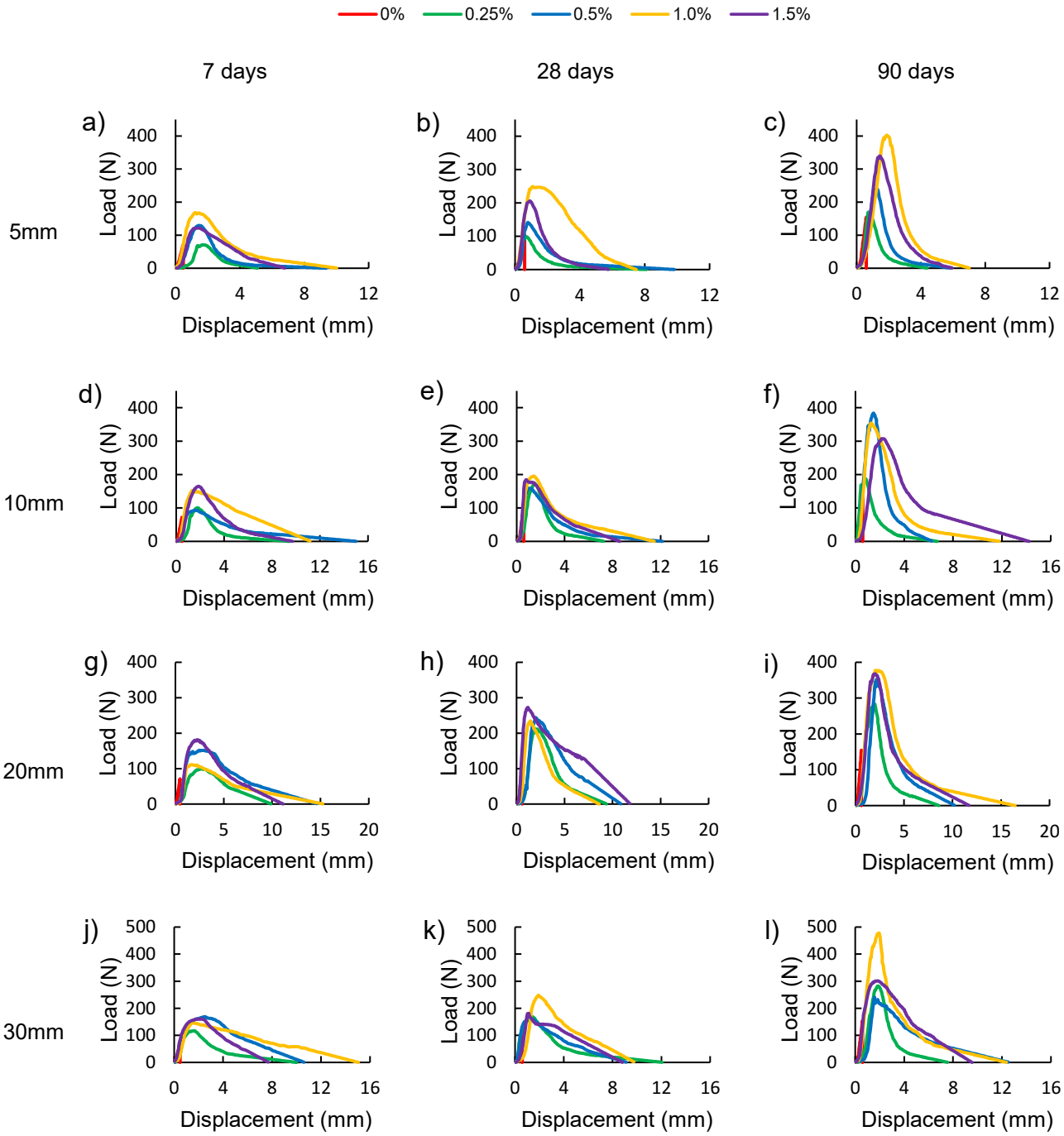

Figure 4.2. Mode-II load-displacement curves of NFR-CPB at different curing times.

The load-displacement curves of NFR-CPB under mode-II loading conditions are illustrated in Figure 4.2. The introduction of hemp fiber affects both the pre-and post-peak response of CPB. Like the mode-I load-displacement behavior, adding hemp fibers

influences the pre-peak slope, enhances the peak resistance, and reinforces the post-peak resistance under mode-II loading conditions. Therefore, hemp fibers are suitable for use as reinforcement materials for CPB. However, it is crucial to identify the different mode-II behavior relative to the counterparts under mode-I loading conditions. Specifically, as the fiber length increases, the rate of change of post-peak resistance becomes smaller, indicating a tougher material at the post-peak stage. A similar evolutionary trend was observed from CPB with various fiber lengths under the mode-I loading condition. This difference implies that fiber length plays a more critical role in the post-peak response under mode-II loading conditions compared to mode-I loading conditions. The improvements in post-peak resistance can be attributed to enhanced fiber-matrix interaction under mode-II loading conditions. This is because, compared with the mode-I loading conditions, mode-II loading conditions can effectively activate both interparticle and particle/fiber friction. As a result, the enhanced fiber-matrix interaction can increase resistance to crack propagation and intensify the crack trajectory's curvature under mode-II loading conditions. Consequently, a tougher NFR-CPB with enhanced post-peak resistance can be obtained under mode-II loading conditions.

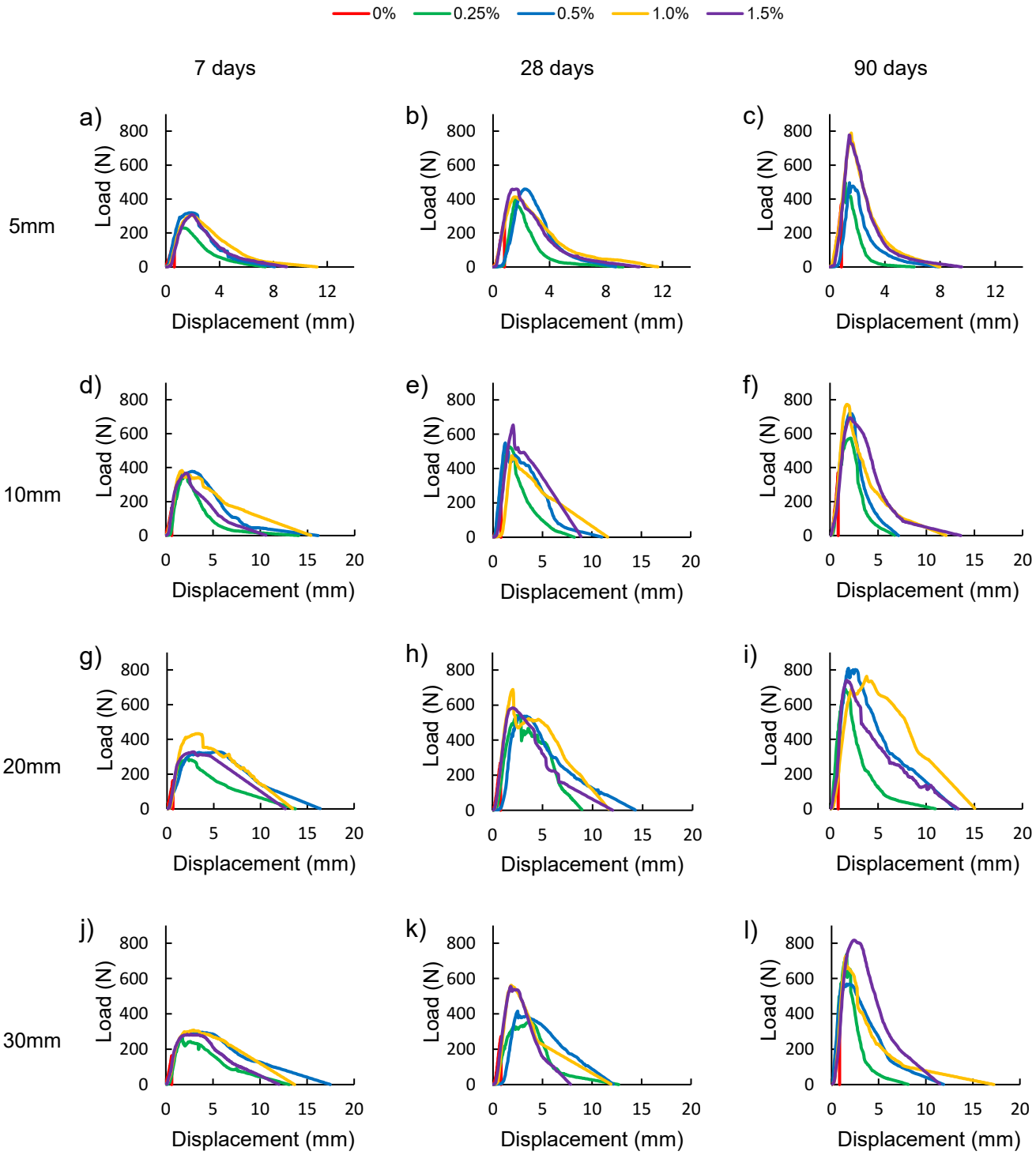

Figure 4.3. Mode-III load-displacement curves of NFR-CPB at different curing times.

The mode-III load-displacement curves of NFR-CPB are presented in Figure 4.3. At the 7-day curing time, the 5mm fiber showed a lower peak load and rapid decline, indicating insufficient crack bridging. The 10mm fiber had a moderate peak load with a brittle response. The 20mm fiber achieved the highest peak load, while the 30mm fiber had a high peak load with a more gradual decline. The pseudo-hardening effect observed under mode-III loading conditions is likely due to higher fiber content and distribution, improving load transfer and crack bridging effects. At 28 days, the 5mm fiber showed increased peak load and moderate decline. The 10mm fiber had a significant peak load increase and gradual decline. The 20mm fiber maintained the highest peak load with ductile behavior, while the 30mm fiber showed similar results to the 20mm but with an extended response. The pseudo-hardening effect is more pronounced, indicating better fiber-matrix interaction and crack bridging. The 90-day results show further enhancements. The 5mm fiber had a higher peak load but remained brittle post-peak. The 10mm fiber exhibited high peak load and ductile behavior. The 20mm fiber had the highest peak load with the most ductile behavior, while the 30mm fiber was comparable to the 20mm but with a gradual decline. The pseudo-hardening effect is most pronounced under the mode-III loading conditions, likely due to the optimal fiber length and curing time enhancing toughness and load transfer. Based on the obtained load-displacement curves under various loading conditions, it can be found that longer fibers (20mm and 30mm) consistently exhibited higher peak loads and more ductile post-peak behaviors than shorter fibers (5mm and 10mm). Hemp fiber effectively improves post-peak behavior due to its ability to bridge cracks and transfer loads even after the matrix begins to fail. The longer fibers provide better crack-bridging capabilities, enhancing toughness and post-

peak resistance. The performance improved with longer curing times, indicating better fiber-matrix bonding and matrix strength.

4.2 Evolutive material stiffness of NFR-CPB

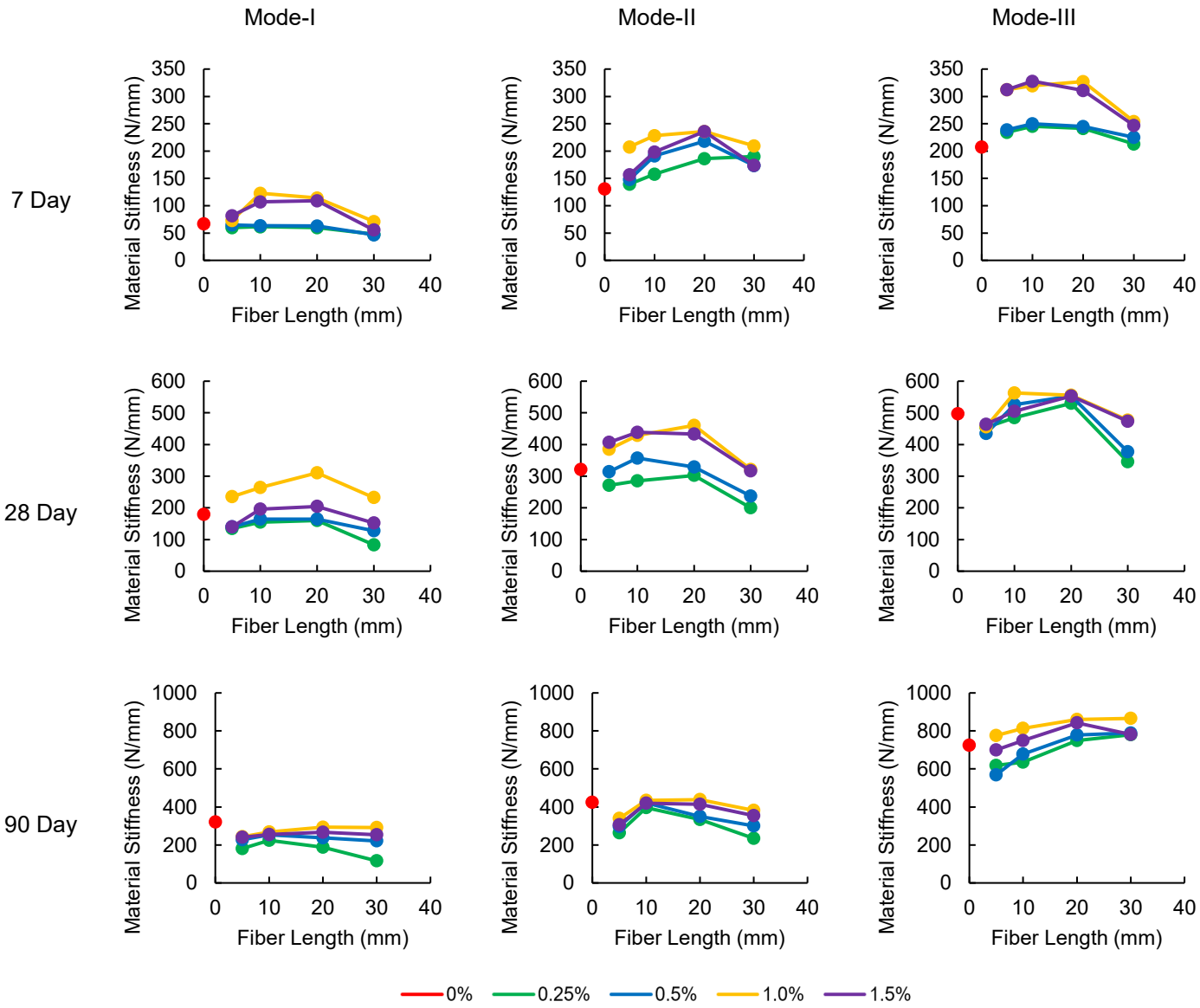

Figure 4.4. Effect of hemp fibers on the evolutive material stiffness of NFR-CPB under different loading conditions.

Figure 4.4 illustrates the effect of hemp fibers on the evolving material stiffness of NFR-CPB under different loading conditions. Using Equation (1.1), the material stiffness of

NFR-CPB was calculated and presented. At the lowest fiber content (0.25%), a trend of decreasing mode-I stiffness with increasing fiber length is observed, suggesting that at this low fiber content, longer fibers may not contribute effectively to stiffness, likely due to insufficient fiber-matrix interaction. As the fiber content increases, material stiffness initially rises with fiber length before declining, indicating an optimal fiber length for each content level. Beyond this optimal length, factors such as fiber aggregation and misalignment may offset the benefits of additional fiber length. For the 28-day NFR-CPB samples, a peak in stiffness improvement is seen compared to the 7-day samples, likely attributed to enhanced water drainage facilitated by the fibers, which increases matric suction. However, by 90 days, this trend reverses, with NFR-CPB samples showing lower stiffness than the control. This could be due to reduced water content limiting the contribution of matric suction to the matrix integrity. Both mode-II and mode-III demonstrate that fiber inclusion enhances stiffness at 7 and 28 days, likely due to fibers facilitating better stress distribution and reducing local stress concentrations.

In mode-II, the 28-day NFR-CPB samples consistently show increased stiffness compared to the control, indicating effective stress transfer facilitated by the fibers. However, by 90 days, there is a noticeable reduction in mode-II stiffness for NFR-CPB compared to control samples. This decline may be attributed to fibers disrupting matrix integrity over time, coupled with the diminished lubricating effect of pore water as it is consumed during hydration. In contrast, under mode-III loading, the 28-day NFR-CPB samples exhibit reduced stiffness, possibly due to the high water content at this stage, which exacerbates particle rotation and impairs the formation of an interlocking particle structure. By 90 days, mode-III stiffness improves significantly compared to mode-II, likely

due to the reduced lubricating effect of pore water, allowing fibers to engage more effectively with the matrix and enhance resistance to complex loading scenarios.

In summary, material stiffness shows a clear time-dependent sensitivity to fiber content and length. The benefits of fiber reinforcement are most pronounced at 28 days, suggesting an optimal period when fibers contribute most to stiffness. However, the long-term effects of fibers on material stiffness (at 90 days) suggest a trade-off between short-term gains and long-term performance, particularly at higher fiber contents. The trends observed at 90 days indicate that the long-term performance of fiber-reinforced CPB may be compromised if fiber content and length are not properly optimized. Understanding the interaction between fibers and the cementitious matrix is crucial for optimizing the mechanical properties of NFR-CPB across all loading modes and over time.

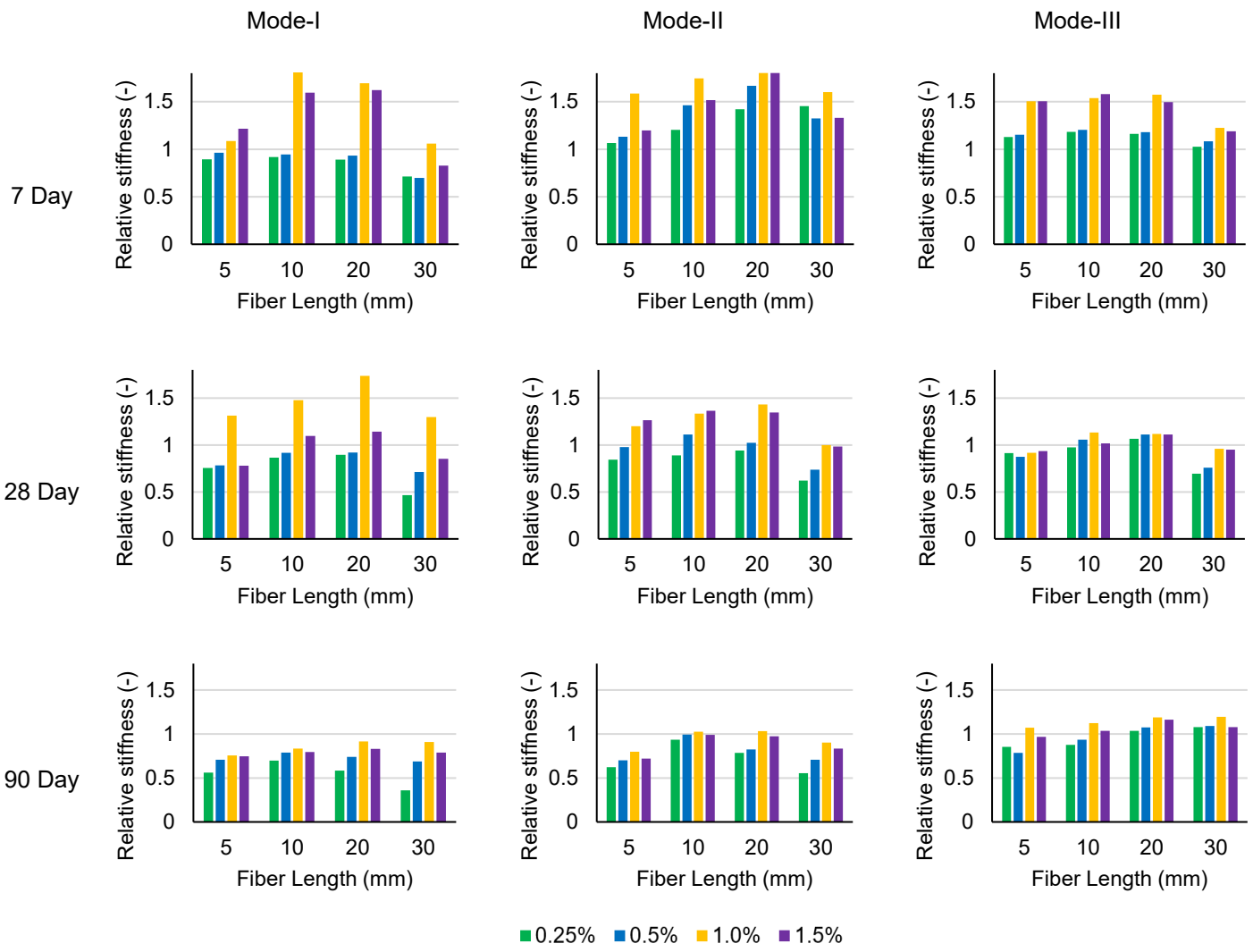

Figure 4.5. Effect of hemp fibers on the relative stiffness of NFR-CPB under different loading conditions.

The effect of hemp fibers on the relative stiffness of NFR-CPB under different loading conditions is illustrated in Figure 4.5. It is important to note the differences in the absolute values of material stiffness under various loading conditions. Comparing relative stiffness, calculated relative to the counterpart of control samples, provides insights into the similarities and differences of material stiffness under various loading conditions. A value of relative stiffness above one indicates that the addition of fibers increases the stiffness of the cementitious matrix relative to the control CPB, suggesting that fibers are beneficial

to the composite's stiffness. Conversely, values below 1 suggest that the addition of fibers decreases the stiffness of the matrix relative to the control, indicating that in these cases, fibers may be detrimental to stiffness or that their potential benefits are not being realized under the given conditions.

The relationship between fiber length and relative stiffness is complex. Although longer fibers are generally expected to improve the bridging effect, the data indicates this is not always true. At 90 days, fiber length seems to reach a limit where further increases do not contribute positively to mode-I relative stiffness, possibly due to issues like fiber aggregation and misalignment within the matrix. This suggests the need for an optimal fiber length that maximizes stress transfer without compromising the composite structure due to excessive fiber length. Fiber content, particularly at levels of 0.5% and 1%, appears to offer a balance that maximizes the benefits of fiber addition, avoiding potential drawbacks like reduced workability and stress concentration. In pure mode-I loading, there is a more pronounced decrease in relative stiffness with the addition of fibers, indicating that the fiber-matrix interaction under tension may require careful optimization to avoid long-term negative effects. On the other hand, mode-II loading shows higher relative stiffness, especially at 28 days, as the fibers effectively contribute to stress distribution by bending around matrix elements. This highlights the beneficial role of fibers in improving stiffness under mode-II conditions.

Mode-III relative stiffness presents the most complex interaction, as the combined shear and tension forces significantly engage the fibers, contributing positively to the matrix's structural integrity. Moreover, mode-III stiffness shows less variation over time than mode-I, suggesting that the fibers provide more consistent reinforcement across curing

periods under these conditions. Overall, the effectiveness of fiber reinforcement in CPB is highly dependent on the mode of stress, fiber length, and content. Neither fiber length nor content universally improves stiffness; these factors must be carefully optimized for each stress mode to achieve the best results. Fiber orientation and mechanical action are particularly important under mode-II and mode-III conditions, and the data supports a targeted approach to fiber reinforcement.

4.3 Evolutive fracture toughness of NFR-CPB

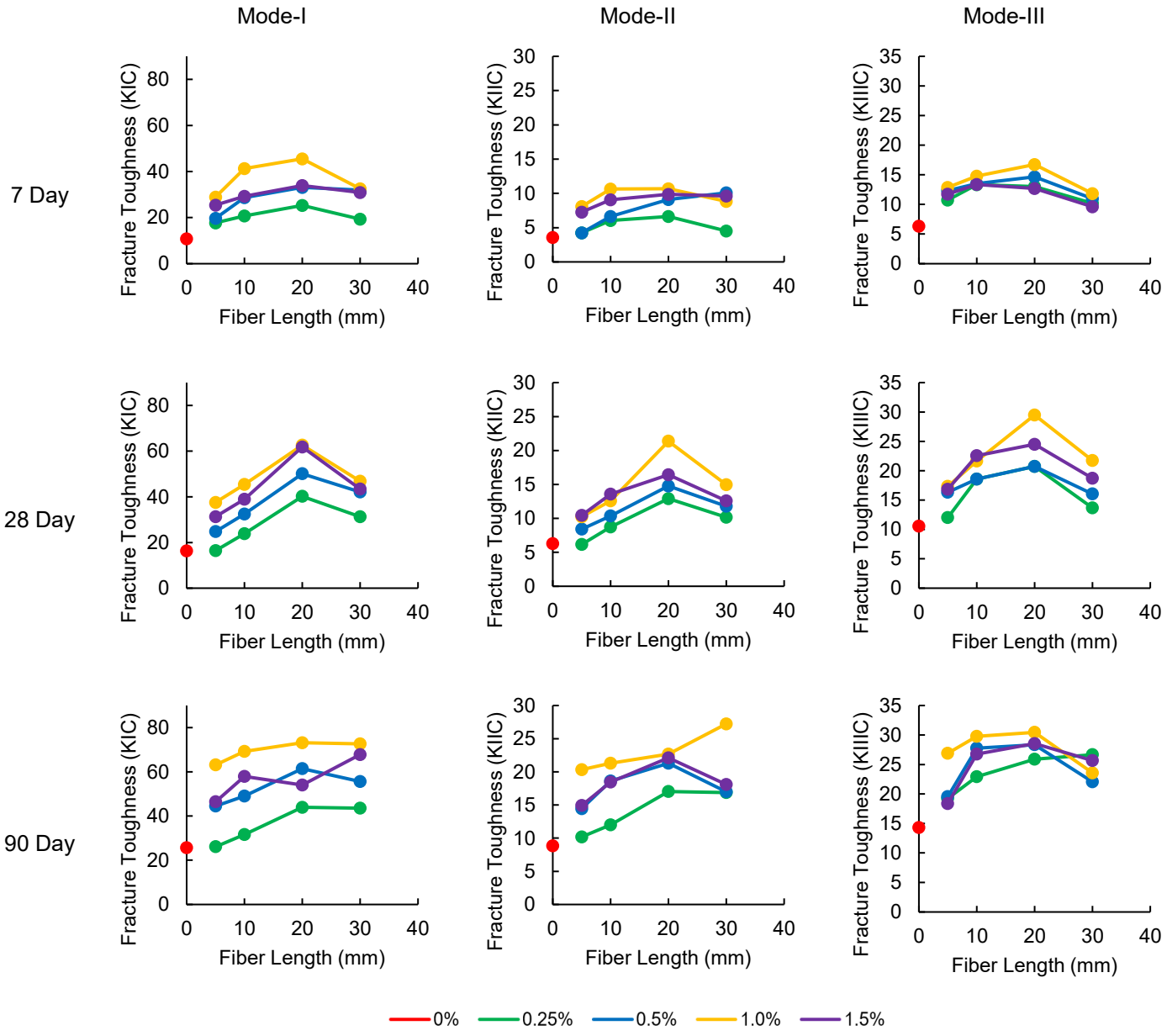

Figure 4.6. Effect of hemp fibers on the evolutive fracture toughness of NFR-CPB under different loading conditions.

Figure 4.6 presents the evolutive fracture toughness of NFR-CPB under different loading conditions. At the early curing stage (7 days), fracture toughness under mode-I loading increases with fiber length, peaking at 20mm for all fiber contents. By 28 days, this peak becomes more pronounced, with the highest fracture toughness observed for 20mm

fibers across all fiber contents, suggesting that longer fibers become more effective as the composite matures. At 90 days, a general trend of increasing fracture toughness with fiber length is observed, except at the 1.5% fiber content, where the trend reverses after 20mm. This indicates that high fiber content may lead to toughness degradation over time. Under mode-II loading, the 7-day fracture toughness generally increases with fiber length, though the trend is less pronounced than in mode-I. The 1.0% fiber content provides the greatest improvement across all lengths, suggesting an optimal fiber content for mode-II loading. By 28 days, the trend becomes more distinct, indicating that the matrix has developed sufficient inherent toughness, thereby increasing the relative impact of fiber length. However, at 90 days, the trends become more varied, with a slight decrease in fracture toughness for longer fibers at 0.5% and 1.0% fiber contents. This suggests a complex interaction between fiber content, fiber length, and the maturing matrix, which requires a balanced approach to optimize toughness.

For mode-III fracture toughness, the 7-day data shows a slight increase or stabilization with fiber length, particularly at 0.5% and 1.0% fiber contents. In contrast, 0.25% and 1.5% show less consistent behavior, reflecting the need for an optimal fiber content that is neither too low nor too high. By 28 days, the trend is like the 7-day results, with 0.5% and 1.0% fiber content continuing to show the best performance across all fiber lengths. This consistency over time supports the idea that there is an optimal fiber content for maximizing toughness. At 90 days, however, the optimal fiber length becomes less apparent for 0.25% and 1.0% fiber contents as fracture toughness increases from 20mm to 30mm, indicating that longer fibers may sometimes be more beneficial in the long term.

A clear trend emerges where intermediate fiber contents (0.5% and 1%) generally perform better across all modes and curing times, indicating that an optimal range of fiber content exists for improving fracture toughness. Over time, the benefit of increasing fiber length diminishes, particularly at the highest fiber content (1.5%), which may be due to issues like fiber clustering or difficulties in dispersion within the matrix. The optimal fiber length for maximizing fracture toughness varies with curing time, with 30mm fibers becoming more effective at 90 days under mode-II loading, likely due to enhanced fiber interlock as the matrix matures. This relationship highlights the importance of optimizing fiber length and content to achieve the desired improvements in fracture toughness. The data suggests that while fiber inclusion generally enhances fracture toughness, maintaining a balance is essential to avoid negative effects, especially with excessive fiber content over longer curing periods.

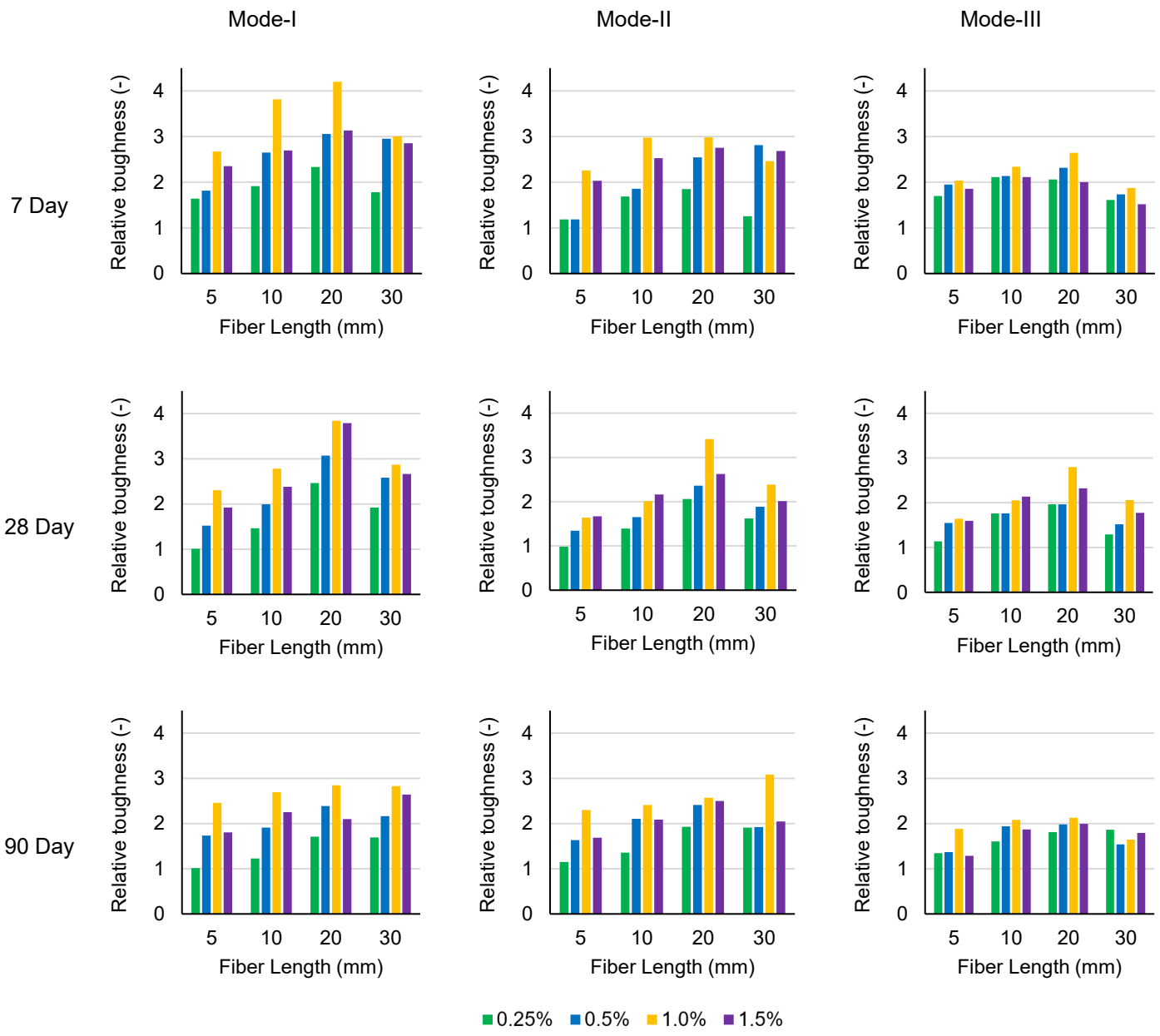

Figure 4.7. Effect of hemp fibers on the relative fracture toughness of NFR-CPB under different loading conditions.

Figure 4.7 shows the relative fracture toughness of NFR-CPB under different loading conditions. As fiber content increases from 0.25% to 1.5%, there is a general trend where adding more fibers enhances fracture toughness relative to the control CPB, supporting the idea that fibers can improve matrix stiffness and strength by bridging cracks and

reinforcing the material. However, the additional fibers no longer increase fracture toughness beyond a certain fiber content, as seen with the 1.5% fibers. This suggests that negative effects such as matrix degradation and uneven stress distribution at higher contents begin to outweigh the benefits of fiber reinforcement.

The variations in relative fracture toughness across the 7, 28, and 90-day data for each fiber length and content highlight the evolving fiber-matrix interactions during cement hydration. The 90-day data provides insights into fiber reinforcement's long-term stability and effectiveness, showing improved relative fracture toughness over time as the fiber-matrix bond strengthens and matures. Fiber length also plays a critical role in fracture toughness improvement, as different lengths exhibit varying efficiencies. This suggests that the bridging effect is length-dependent, with optimal fiber length crucial for performance. Shorter fibers (5mm) may not adequately span cracks, resulting in less effective stress transfer, while longer fibers (30mm) might encounter distribution issues within the matrix or may curl and clump, reducing their effectiveness.

Under mode-I loading conditions, effective stress transfer in pure tension requires good fiber-matrix adhesion. There may be an optimal fiber content that maximizes adhesion without introducing defects in the matrix. For mode-II relative fracture toughness, additional fiber content enhances bending resistance, but the efficiency varies with fiber length, indicating complex interactions within the matrix that affect toughness. In mode III, fracture toughness exhibits a more complex behavior. Fiber content up to 1.0% generally improves fracture toughness, as this mode benefits from aggressive fiber engagement through twisting and pullout actions, indicating strong fiber-matrix interactions.

Overall, the effectiveness of fiber reinforcement in CPB is highly dependent on fiber content, length, curing time, and the type of stress. An optimal fiber content range (between 0.5% and 1.0%) maximizes the benefits across all modes and time frames, balancing reinforcement and the negative effects of excessive fiber content. Fiber length also plays a crucial role, with neither too short nor too long fibers being universally beneficial. Each stress mode requires a careful selection of fiber length and content to improve material stiffness and overall performance.

4.4 Evolutive fracture energy of NFR-CPB

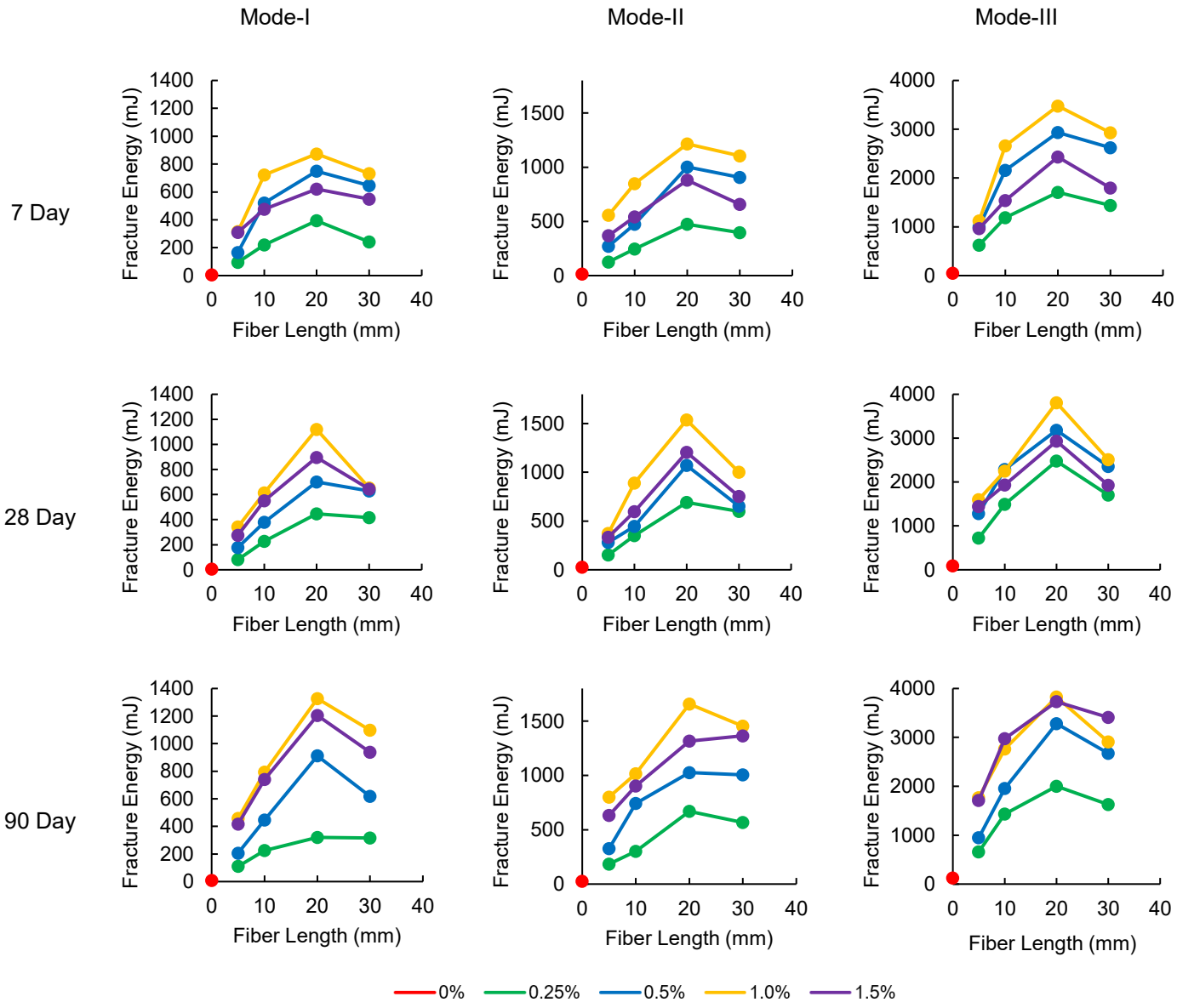

Figure 4.8. Effect of hemp fibers on the fracture energy of NFR-CPB under different loading conditions.

Figure 4.8 shows the effect of hemp fibers on the fracture energy of NFR-CPB under different loading conditions. In mode-I at 7 days, there is a clear upward trend in fracture energy with increasing fiber length, particularly up to 20mm, indicating that longer fibers enhance energy dissipation under tensile stress. As curing time increases, the improvement in mode-I fracture energy becomes more evident, confirming the critical role

of curing time in developing the material's energy dissipation capabilities. This suggests that the effectiveness of fiber reinforcement is closely tied to the extent of cement hydration. In older CPB, the improvement in fracture toughness becomes more pronounced with longer fibers. Specifically, the enhancement in fracture energy becomes more sensitive to fiber content as the fiber length increases to 20mm and 30mm. The results suggest that fiber length plays a more significant role in mode-I fracture energy than fiber content. However, when fiber length reaches 30mm, fracture energy decreases compared to 20mm, indicating an optimal fiber length (20mm) for improving fracture energy. Increasing fiber content up to 1% improves fracture energy, while 1.5% has a negative effect, reducing the CPB's ability to dissipate strain energy. Introducing fibers into the CPB matrix creates a fiber-matrix interfacial transition zone with high porosity and weak adhesion. When too many fibers are used, their negative influence on the matrix offsets the reinforcement effect. Thus, an optimal fiber content of 1% exists, which maximizes the improvement in fracture energy.

Mode-II fracture energy exhibits a similar fiber length and content sensitivity to mode-I. In-plane shear fracture energy increases with fiber content up to 1% but decreases at 1.5%. The highest fracture energy is observed with 20mm fibers, suggesting that a combination of 20mm fiber length and 1% fiber content optimally enhances fracture energy under mode-II loading. The continuous improvement in mode-II fracture energy with curing time highlights the critical role of cement hydration in developing shear fracture energy. This is due to the accumulation of hydration products, such as calcium silicate hydrates (C-S-H), which strengthen the adhesion between fibers and tailings over time. Compared to mode-I, the improvement in mode-II fracture energy is more pronounced,

suggesting additional contributors to shear fracture energy beyond cement hydration, such as enhanced particle friction and interlocking between fibers and tailings. Introducing fibers increases matrix porosity, which improves hydraulic conductivity and local water drainage. Consequently, CPB with higher fiber content experiences lower water content and reduced pore-water lubrication, leading to stronger particle friction and interlocking structures under mode-II loading. This fiber reinforcement and particle friction combination contributes more significantly to fracture energy development than in mode-I.

For mode-III fracture energy, there is a noticeable increase with fiber length at 7 days, especially for the longest fibers, suggesting that fiber length has a more pronounced effect under combined loading conditions in the early stages. This trend continues at 28 days, with longer fibers contributing to higher fracture energy, indicating that fiber length plays a significant role in energy absorption as the composite cures. By 90 days, the increase in fracture energy with fiber length becomes even more pronounced, showing that under mode-III loading, fibers effectively bridge cracks and enhance the composite's energy absorption capacity over time.

Across all loading modes, the effect of fiber length on fracture energy becomes more pronounced at later curing stages, particularly in mode-III. This may reflect how fibers interact with the matrix under different loading conditions. While there is no dramatic variation in fracture energy with fiber length at 7 days, there is a slight trend toward increased energy absorption with longer fibers as curing extends to 28 and 90 days. The data suggests that while fiber length influences fracture energy, curing time and the

loading mode are critical factors. Longer fibers appear beneficial in combined loading conditions and at later curing stages.

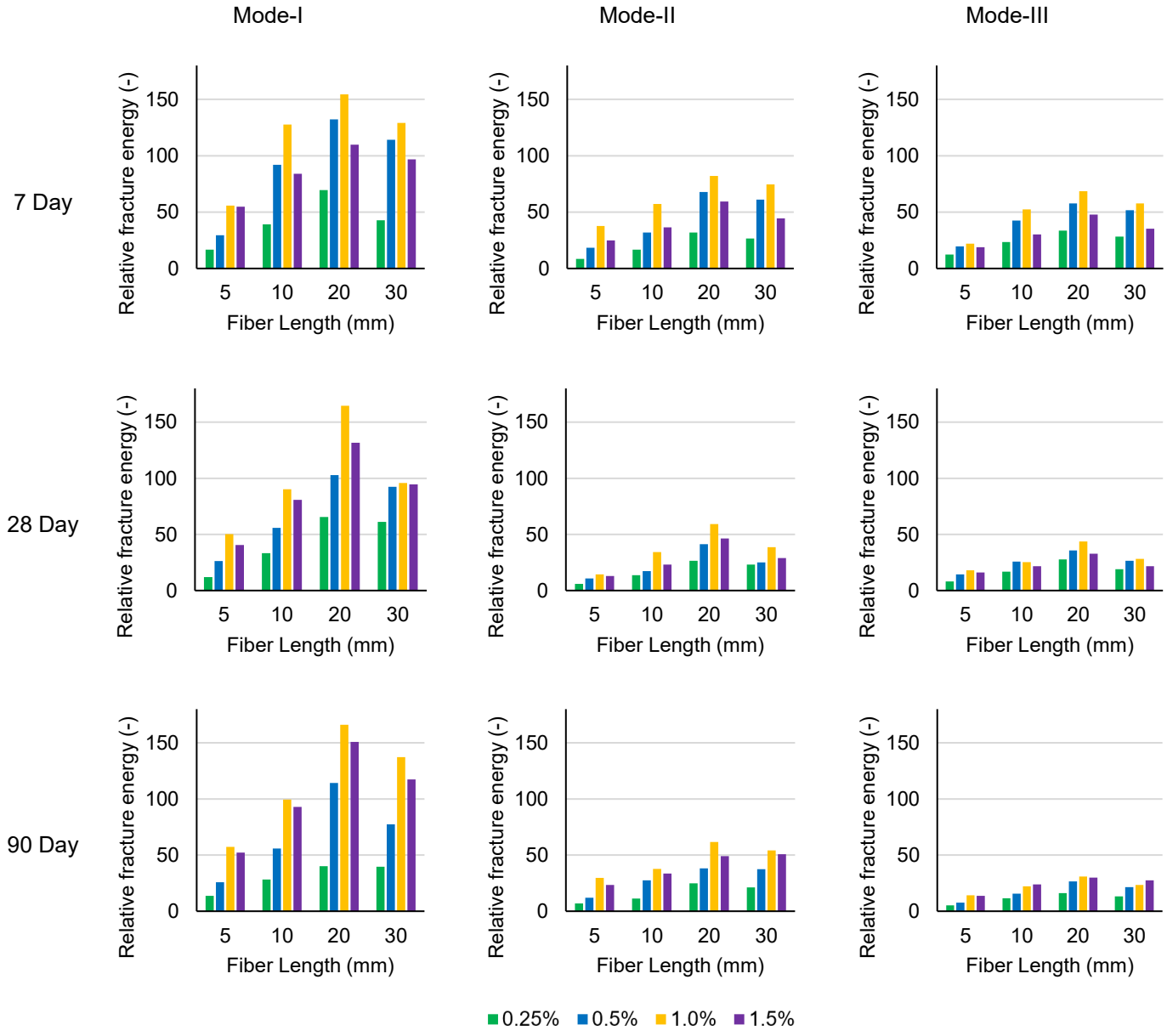

Figure 4.9. Effect of hemp fibers on the relative fracture energy of NFR-CPB under different loading conditions.

The evolution of relative fracture energy in mode-II and mode-III loading conditions reveals distinct patterns in their response to variations in fiber length and curing periods,

as depicted in Figure 4.9. Mode-I relative fracture energy exhibits the greatest sensitivity to changes in fiber length across the different curing periods. This sensitivity can be attributed to the nature of mode-I loading, which is characterized by uniaxial tension that places fibers in direct alignment with the tensile force, allowing them to contribute more effectively to the fracture energy of the composite. During the 7-day curing period, the matrix is not fully cured, and the contribution of fibers to the fracture energy can be significant. The fibers can effectively bridge micro-cracks that develop during the early stages of curing, and longer fibers may be particularly beneficial due to their increased bridging capability. This heightened sensitivity can be attributed to the nature of mode-I loading, characterized by uniaxial tension. In this scenario, fibers are directly aligned with the tensile force, allowing them to contribute more effectively to the composite's fracture energy. When the matrix is still developing, the contribution of fibers to fracture energy is significant. Fibers can bridge micro-cracks that form early in curing, with longer fibers offering enhanced bridging capabilities.

The sensitivity observed in mode-I fracture energy stems from fiber length's direct impact on stress transfer and crack propagation in tensile-dominated failure. As the matrix continues to cure and gains stiffness and strength, the role of fiber reinforcement may shift. Fibers continue to significantly contribute to fracture energy even in this later stage, particularly as the matrix becomes more brittle. Longer fibers remain active in bridging cracks, becoming even more crucial as the matrix stiffens. The sensitivity of mode-I fracture energy suggests that fiber alignment with the tensile force is critical for improving toughness. By the 90-day curing period, the matrix is expected to have achieved most of its strength, potentially altering the relative impact of fibers. However, the sensitivity to

fiber length persists as fibers continue to arrest crack growth in a mature, less ductile matrix. In this stage, the ability of fibers to enhance toughness becomes more pronounced, and their length plays a key role in the composite's ability to absorb energy before fracture. In mode-II relative fracture energy, the data shows a general increase with longer fibers and higher fiber content, especially noticeable during the 28-day curing period. This suggests that shear forces in mode-II benefit from fiber reinforcement, as fibers provide an interlocking mechanism that enhances shear resistance. During the early 7-day curing period, the matrix is still developing, and fibers play a crucial role in bridging cracks caused by shear stress. As the matrix strengthens at 28 and 90 days, the combined effects of matrix stiffening and fiber reinforcement result in higher fracture energy. Increased fiber content, particularly at 1.0% and 1.5%, significantly improves fracture energy, indicating that a higher fiber density effectively distributes shear forces across the composite.

In contrast, mode-III relative fracture energy shows a more modest increase with fiber length and content than mode-II. However, noticeable improvements in fracture energy at 1.0% and 1.5% fiber content are still evident, particularly at the 28-day curing period. In mode-III, fibers primarily hinder the progression of out-of-plane cracks by creating a three-dimensional network that resists tearing. As curing progresses, the increased matrix strength from hydration further enhances the fibers' ability to contribute to fracture resistance. Overall, the evolution of relative fracture energy demonstrates the complex interaction between fiber length, content, and curing time under different loading modes. While mode-I demonstrates the highest sensitivity to fiber length, both mode-II and mode-

III benefit from optimal fiber reinforcement, particularly at higher fiber contents and longer curing times.

4.5 Microstructure analysis of NFR-CPB

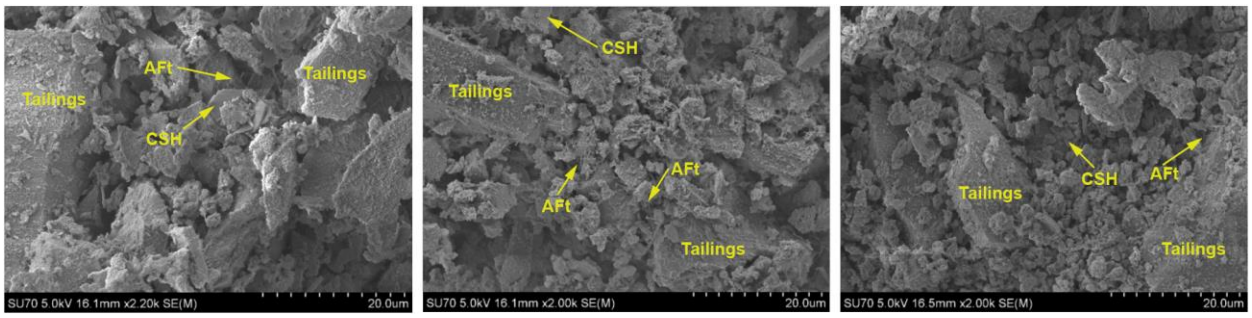

Figure 4.10. SEM images of control CPB samples without fiber reinforcement: (a) 7 days, (b) 28 days, and (c) 90 days.

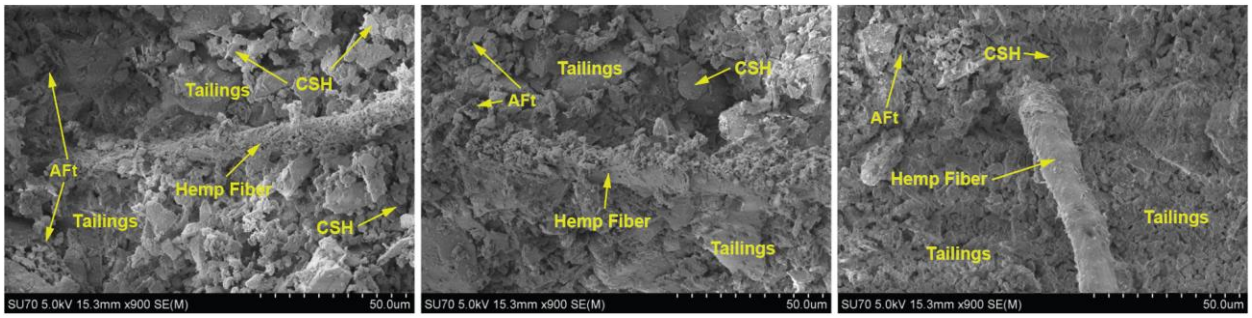

Figure 4.11. SEM images of NFR-CPB samples with fiber reinforcement: (a) 7 days, (b) 28 days, and (c) 90 days.

The SEM images of control CPB samples at different curing times (7 days, 28 days, and 90 days), as shown in Figure 4.10, provide valuable insights into the microstructural evolution of the material over time. At 7 days, the CSH appears in a relatively initial formation stage, with a less dense morphology, indicating the early stages of hydration. Aluminate Ferrite Monosulfate (AFt) suggests ongoing hydration reactions, with needle-like structures indicative of ettringite, which forms rapidly during the early stages of cement hydration. Tailings particles are still prominently visible, indicating that the binding

between the cement hydration products and the tailings is still developing. By 28 days, the CSH structures are more pronounced and denser than the 7-day sample, suggesting significant progress in the hydration process and leading to a more interconnected matrix. The AFt structures are still present, though they might be more integrated into the matrix as hydration progresses, with an increased density of hydration products surrounding these needle-like formations more closely. Tailings particles appear more embedded within the matrix, indicating improved bonding and reduced porosity, showing a progression towards a more cohesive microstructure. At 90 days, the CSH has formed a very dense and well-connected network, suggesting that the hydration process has substantially advanced, with the CSH gel filling most of the voids and contributing to the strength and stability of the CPB. The presence of AFt structures is less prominent, which could be due to their conversion into other hydration products over time. The microstructure shows fewer distinct needle-like formations, implying ongoing secondary hydration reactions. The tailings particles are almost completely enveloped by the hydration products, indicating a mature and stable microstructure, with the interaction between tailings and hydration products at its peak, providing maximum strength and durability to the CPB.

The SEM images of NFR-CPB samples at different curing times (7 days, 28 days, and 90 days) are presented in Figure 4.11. At 7 days, the hemp fibers are visibly integrated within the matrix, but the bonding appears to be in its initial stages. The fibers are surrounded by a less dense CSH gel and tailings particles, indicating the early stages of hydration. The CSH structures are less dense and more amorphous, suggesting the early formation of hydration products. AFt indicates ongoing hydration reactions, with needle-like

structures typical of ettringite forming rapidly during the initial hydration stages. The tailings particles are still quite prominent and not fully encapsulated by the hydration products, showing that the binding process is still developing. By 28 days, the hemp fibers show better integration within the CPB matrix. The surrounding CSH is denser, indicating significant progress in the hydration process. The CSH structures are more pronounced and interconnected, forming a denser matrix that enhances the overall strength of the material. The AFt structures are still present but appear more integrated into the matrix. The density of hydration products around these structures has increased. The tailings particles are more embedded within the matrix, showing improved bonding and reduced porosity. This indicates a progression towards a more cohesive microstructure. At 90 days, the hemp fibers are well-embedded within a very dense and well-connected CSH network, suggesting a mature hydration process. The CSH has formed a dense and stable network, filling most of the voids and significantly contributing to the strength and stability of the CPB. The AFt structures are less prominent, possibly due to their conversion into other hydration products over time. The matrix shows fewer distinct needle-like formations, implying ongoing secondary hydration reactions. The hydration products almost completely envelop the tailings particles, indicating a mature and stable microstructure. The interaction between the tailings and hydration products is at its peak, providing maximum strength and durability to the CPB.

Over the 90 days, the SEM images reveal a clear progression in the microstructure of the NFR-CPB samples. At 7 days, there are early stages of hydration with initial CSH formation and prominent AFt and tailings particles. By 28 days, hydration products are significantly developed, leading to a denser and more interconnected matrix. At 90 days,

the hydration process matures, resulting in a very dense, well-bonded, and stable microstructure with embedded hemp fibers. These observations highlight the role of curing time in developing the microstructural properties that contribute to the mechanical strength and durability of CPB and NFR-CPB. The increasing density and integration of hydration products over time demonstrate the effectiveness of hemp fiber reinforcement and the curing process in enhancing the material properties of CPB.

4.6 Discussion

At early curing stages, such as 7 and 28 days, the matrix is still relatively weak and has not yet achieved full strength. During this period, the matrix is more susceptible to microstructural changes and less able to resist the internal stresses and potential "cutting" effect caused by fiber movements within the composite. When fibers are added to the matrix, they can create internal micro-cracks as they attempt to bridge the gaps between cracks or when they are pulled out under load. This "cutting" effect can be particularly pronounced with longer or higher content fibers that exert greater force on the surrounding material. Since the matrix has not fully hardened at 7 and 28 days, it cannot sustain this cutting effect efficiently, leading to a decrease in fracture energy, as observed in some data trends.

By the time the matrix reaches 90 days, the material has generally undergone significant hydration and has developed increased strength and stiffness. At this stage, the matrix can better integrate the fibers and resist the internal forces they create. However, the contribution of matric suction, which is the tension within the pore water of the matrix due to capillary action and can aid in holding the matrix together, becomes weaker over time. As the matrix continues to cure, the pore structure changes and becomes less able to

generate capillary forces. Furthermore, the overall water content decreases as it is consumed by ongoing hydration reactions, which reduces the matric suction effect. Therefore, while at 90 days, the matrix is stronger and more rigid, potentially making it more effective at transferring loads to the fibers, the reduced matric suction could limit the overall contribution of the fibers to the toughness of the matrix. In other words, while the fibers can still bridge cracks and provide reinforcement, the diminished matric suction means that the matrix provides less overall toughness, and the fibers' role becomes more critical. This could explain why the trends in fracture energy with fiber length become more pronounced at 90 days. The matrix's reduced ability to contribute to toughness through matric suction means that the fibers' ability to bridge and hold together the matrix plays a greater role.

The sensitivity of mode-III fractures to fiber length is linked to this loading mode's unique stress and deformation patterns. Mode-III loading subjects the composite material to out-of-plane shear stresses, which induce rotational or twisting forces that significantly differ from mode-I or mode-II loading. Longer fibers within a cement-based matrix contribute more effectively to mechanical interlocking, a vital mechanism for resisting rotational forces under mode-III loading conditions. This interlocking allows the fibers to engage with the matrix material more efficiently, providing superior resistance to the twisting motions that lead to fractures. Shorter fibers may not span across the matrix sufficiently to offer a comparable level of mechanical interlocking, thus diminishing their ability to counteract twisting fractures. Fiber orientation and distribution become particularly significant under mode-III loading conditions. Longer fibers have a greater chance of intersecting potential fracture planes at multiple points, thereby enhancing their ability to

resist the complex stresses induced by twisting. This mode is inherently less sensitive to fiber reinforcement due to the complex nature of the tearing forces that do not align fibers as effectively as tensile, or shear forces. The distribution of these fibers throughout the matrix is also critical; longer fibers are more likely to be oriented in ways that provide resistance across various planes of potential fractures, leading to a more resilient composite structure.

Stress transfer is another factor in which fiber length plays an important role. The ability of fibers to transfer stress across their length can reduce stress concentrations within the matrix. Longer fibers enable a more extensive area for stress distribution, necessitating more energy to initiate and propagate a crack. This distribution is especially crucial in mode-III loading, where the multidirectional stress state can lead to more unpredictable crack paths. Furthermore, the failure mechanism of fibers under mode-III stresses can experience either pull-out or rupture. Longer fibers are typically more prone to rupturing rather than being pulled out, as the latter is a less energy-consuming process. This characteristic means that longer fibers, when subjected to mode-III loading, can absorb more energy before failing, which directly contributes to the increased toughness of the material. The ability of fibers to bridge cracks is also essential in resisting fractures. In mode-III, where cracks can appear due to twisting loads, longer fibers excel in bridging these openings within the matrix, effectively holding together parts of the material that might otherwise separate. This crack-bridging capacity of longer fibers highlights their significance in enhancing fracture energy absorption in mode-III. Lastly, the deformation behavior under mode-III loading involves rotational movement within the matrix and fibers.

Longer fibers can accommodate a greater degree of twisting without failing, allowing them to absorb more energy exerted by twisting loads before the onset of material failure.

In summary, the complex interplay of mechanical interlocking, stress transfer, orientation, and crack bridging explains why mode-III fractures are particularly sensitive to fiber length. However, it's important to recognize that there may be an optimal length for fibers in mode-III fractures. Beyond this optimal point, the benefits may plateau or even reverse due to practical issues such as fiber entanglement or challenges in achieving uniform dispersion within the matrix, highlighting the need for careful optimization of fiber length in composite materials.

Chapter 5 Conclusions and Recommendations

5.1 Conclusions

This study aimed to investigate the fracture behavior of NFR-CPB under mode-I, mode-II, and mode-III loading conditions, focusing on the effects of hemp fiber content and fiber length. The comprehensive experimental program consists of mechanical testing, including semicircular bend (SCB) tests, end-notch disk bend (ENDB) tests, and microstructural analysis using scanning electron microscopy (SEM). The findings provide valuable insights into the mechanical performance and fracture properties of NFR-CPB, contributing to the advancement of backfill technology in underground mining applications.

1. The inclusion of hemp fibers in CPB affects both pre- and post-peak behaviors under mode-I loading. It increases peak load resistance, with effectiveness dependent on fiber length and content. CPB with 20mm fibers achieved the highest peak load and ductility. Over 20mm fibers showed reduced tolerance to displacement at advanced curing times, highlighting the influence of curing time on NFR-CPB.
2. Hemp fibers in CPB under mode-II loading improve load-displacement behavior, increasing peak resistance and post-peak toughness. Fiber length significantly affects post-peak behavior, enhancing fiber-matrix interaction, crack resistance, and curvature. This increases shear resistance and contributes to CPB integrity under field loading conditions.
3. The mode-III load-displacement curves of NFR-CPB show that longer fibers (20mm and 30mm) consistently achieve higher peak loads and more ductile post-peak

behavior than shorter fibers (5mm and 10mm). Hemp fibers improve post-peak behavior by enhancing crack bridging and load transfer. Longer curing times further enhance performance due to improved fiber-matrix bonding and matrix strength.

4. Hemp fibers affect the material stiffness of NFR-CPB under various loading conditions, with an optimal fiber length existing for each fiber content. Stiffness improves at 28 days due to better stress distribution and water drainage but decreases at 90 days, indicating potential long-term performance trade-offs.
5. Hemp fibers impact the relative stiffness of NFR-CPB differently across loading conditions. Optimal fiber length and content are crucial, with 0.5% and 1% being effective. The mode-II and mode-II stiffness improvement becomes more obvious than mode-I ones, showing the need for targeted reinforcement strategies.
6. Using hemp fibers increases NFR-CPB fracture toughness, peaking with 20mm fibers at 7 and 28 days. At 90 days, longer fibers still help, except at 1.5% content. Optimal fiber content (0.5%-1%) improves performance, while excessive content can degrade fracture toughness over curing time.
7. Hemp fibers improve the relative fracture toughness of NFR-CPB, peaking at 1.0% fiber content. Each stress mode requires specific fiber length and content for best performance, with 0.5%-1.0% fiber content generally being the most effective.
8. Hemp fibers enhance NFR-CPB fracture energy; adopting 20mm fiber length and 1% fiber content can maximize fiber reinforcement in the development of fracture energy. Improvements are more pronounced with increased curing time, particularly under mode-III loading. Excessive fiber content (1.5%) reduces effectiveness.

9. Relative fracture energy in mode-II and mode-III loading conditions varies with fiber length and curing periods. Mode-I relative fracture energy is most sensitive to fiber length. Mode-II relative fracture energy benefits from fiber reinforcement, especially at 28 days. Mode-III relative fracture energy shows modest increases with longer fibers and higher fiber content.
10. SEM observations revealed that hemp fibers form a more compact and interlocked microstructure, enhancing the overall mechanical performance of the CPB. Additionally, the incorporation of hemp fibers promoted the formation of calcium silicate hydrate (C-S-H) and ettringite (Aft) products, further contributing to the improved strength and durability of the material.

5.2 Recommendations for future work

Based on this study's findings, several recommendations are proposed for future research to advance the understanding and application of NFR-CPB further. Firstly, investigate the long-term durability and performance of NFR-CPB under various environmental conditions, including exposure to moisture, temperature fluctuations, and chemical interactions. Conduct field trials to evaluate the performance of NFR-CPB in real underground mining conditions. Implement monitoring systems to assess the long-term behavior and stability of the backfill material. Explore the effects of different types of natural fibers, fiber hybridization, and varying fiber contents and lengths to determine the optimal combination for specific mining conditions. Perform a comprehensive economic and environmental impact analysis using NFR-CPB compared to traditional backfill methods. Assess the cost-effectiveness and sustainability of the proposed technology. Develop advanced numerical models to simulate the fracture behavior and mechanical

performance of NFR-CPB. Validate the models with experimental data to predict NFR-CPB behavior under different loading scenarios and optimize the design process. Investigate the use of alternative binders, such as geopolymer or supplementary cementitious materials, in combination with natural fibers to enhance the sustainability and performance of CPB. By addressing these areas in future research, implementing NFR-CPB can be further optimized, leading to safer and more efficient underground mining operations. The insights gained from this study provide a solid foundation for the continued development and application of CPB technology in the mining industry.

References

1. Abbas S, Soliman AM, Nehdi ML. Exploring mechanical and durability properties of ultra-high performance concrete incorporating various steel fiber lengths and dosages. Construction and Building Materials. 2015;75:429-441.
2. Abdalla JA, Thomas BS, Hawileh RA. Use of hemp, kenaf and bamboo natural fiber in cement-based concrete. Materials Today: Proceedings. 2022;65(Part 2):2070-2072.
3. Ahmed ATMF, Islam MZ, Mahmud MS, Sarker ME, Islam MR. Hemp as a potential raw material toward a sustainable world: a review. Heliyon. 2022 Jan 13;8(1):e08753.
4. Ahmad J, Majdi A, Deifalla AF, Ben Kahla N, El-Shorbagy MA. Concrete reinforced with sisal fibers (SSF): overview of mechanical and physical properties. Crystals. 2022;12(7):952.
5. Ahmad J, Zhou Z, Deifalla AF. Structural properties of concrete reinforced with bamboo fibers: a review. Journal of Materials Research and Technology. 2023;24:844-865.
6. Ahmad W, Farooq SH, Usman M, et al. Effect of coconut fiber length and content on properties of high strength concrete. Materials (Basel). 2020;13(5):1075.
7. Aliha MRM, Akhondi Sh. Determination of mode III fracture toughness for different materials using a new designed test configuration. Materials & Design. 2015;86:863-871.

8. Aznar-Sánchez JA, Velasco-Muñoz JF, Belmonte-Ureña LJ, Manzano-Agugliaro F. Innovation and technology for sustainable mining activity: A worldwide research assessment. Journal of Cleaner Production. 2019;221:38-54.
9. Balagopal V, Panicker AS, Arathy MS, Sandeep S, Pillai SK. Influence of fibers on the mechanical properties of cementitious composites - a review. Materials Today: Proceedings. 2022;65(Part 2):1846-1850.
10. Banthia N, Gupta R. Influence of polypropylene fiber geometry on plastic shrinkage cracking in concrete. Cement and Concrete Research. 2006;36(7):1263-1267.
11. Bažant ZP, Oh BH. Crack band theory for fracture of concrete. Matériaux et Construction. 1983;16:155-177.
12. Benzaazoua M, Fall M, Belem T. A contribution to understanding the hardening process of cemented pastefill. Minerals Engineering. 2004;17(2):141-152.
13. Bentur A, Mindess S. Fibre Reinforced Cementitious Composites. 2nd ed. CRC Press; 1990.
14. Bittner CM, Oettel V. Fiber reinforced concrete with natural plant fibers—investigations on the application of bamboo fibers in ultra-high performance concrete. Sustainability. 2022;14(19):12011.
15. Blowes DW, Reardon EJ, Jambor JL, Cherry JA. The formation and potential importance of cemented layers in inactive sulfide mine tailings. Geochimica et Cosmochimica Acta. 1991;55(4):965-978.
16. Buathong P, Chompoorat T, Jongpradist P, Chen X, Jamsawang P. Effect of palm fiber reinforcement on the unconfined compressive performance of cement-treated sand. Sustainability. 2023;15:8607.

17. Chen X, Jiao H, Liu J, et al. The influence of multi-size basalt fiber on cemented paste backfill mechanical properties and meso-structure characteristics. Minerals. 2023;13(9):1215.
18. Chen X, Shi X, Zhang S, et al. Fiber-reinforced cemented paste backfill: the effect of fiber on strength properties and estimation of strength using nonlinear models. Materials (Basel). 2020;13(3):718.
19. Chen X, Shi X, Zhou J, Yu Z. Influence of polypropylene fiber reinforcement on tensile behavior and failure mode of tailings cemented paste backfill. IEEE Access. 2019;7:69015-69026.
20. Chompoorat T, Likitlersuang S, Buathong P, Jongpradist P, Jamsawang P. Flexural performance and microstructural characterization of cement-treated sand reinforced with palm fiber. Journal of Materials Research and Technology. 2023;25:1570-1584.
21. Chakilam S, Cui L. Effect of polypropylene fiber content and fiber length on the saturated hydraulic conductivity of hydrating cemented paste backfill. Construction and Building Materials. 2020;262:120854.
22. Dufresne A. Cellulose nanomaterial reinforced polymer nanocomposites. Current Opinion in Colloid & Interface Science. 2017;29:1-8.
23. Dupont D, Vandewalle L. Distribution of steel fibres in rectangular sections. Cement and Concrete Composites. 2005;27(3):391-398.
24. Elfordy S, Lucas F, Tancret F, Scudeller Y, Goudet L. Mechanical and thermal properties of lime and hemp concrete (“hempcrete”) manufactured by a projection process. Construction and Building Materials. 2008;22(10):2116-2123.

25. Fang K, Cui L. Experimental investigation of evolutive mode-I and mode-II fracture behavior of fiber-reinforced cemented paste backfill: effect of curing temperature and curing time. Frontiers of Structural and Civil Engineering. 2023;17(2):256-270.
26. Festugato L, Fourie A, Consoli NC. Cyclic shear response of fibre-reinforced cemented paste backfill. Géotechnique Letters. 2013;3(1):5-12.
27. Festugato L, Menger E, Benezra F, Kipper EA, Consoli NC. Fibre-reinforced cemented soils compressive and tensile strength assessment as a function of filament length. Geotextiles and Geomembranes. 2017;45(1):77-82.
28. Gao B, Cao S, Yilmaz E. Effect of content and length of polypropylene fibers on strength and microstructure of cementitious tailings-waste rock fill. Minerals. 2023;13(2):142.
29. Ghirian A, Fall M. Strength evolution and deformation behaviour of cemented paste backfill at early ages: effect of curing stress, filling strategy and drainage. International Journal of Mining Science and Technology. 2016;26(5):809-817.
30. Gou M, Zhou L, Then N. Utilization of tailings in cement and concrete: a review. Science and Engineering of Composite Materials. 2019;26(1):449-464.
31. Guo H, Jiang L, Tao J, Chen Y, Zheng Z, Jia B. Influence of a hybrid combination of steel and polypropylene fibers on concrete toughness. Construction and Building Materials. 2021;275:122132.
32. Guowei M, Zhijian L, Xiawei Y, Lijie G. Macro-meso experiment of fiber-reinforced cement paste filling material. Journal of Beijing University of Technology. 2016;42(3):406-412.

33. Hannant, D. J., Fiber Cements and Fiber Concretes, John. Wiley & Sons, New York, 1978.
34. Hou Y, Yang K, Yin S, et al. Enhancing workability, strength, and microstructure of cemented tailings backfill through mineral admixtures and fibers. Journal of Building Engineering. 2024;84:108590.
35. Jafari M, Shahsavari M, Grabinsky M. Drained triaxial compressive shear response of cemented paste backfill (CPB). Rock Mechanics and Rock Engineering. 2021;54:3309–3325.
36. Jiao L, Su M, Chen L, Wang Y, Zhu H, Dai H. Natural cellulose nanofibers as sustainable enhancers in construction cement. Plos One. 2016;11(12).
37. Jie Wang, Qinjun Yu, Zhuozhi Xiang, Jianxin Fu, Leiming Wang, Weidong Song. Influence of basalt fiber on pore structure, mechanical performance and damage evolution of cemented tailings backfill. Journal of Materials Research and Technology. 2023;27:5227-5242.
38. Jin J, Li C, Yuan S, Sun Q, Yang H. Effect of fiber on early strength and interface stiffness of cemented tailings backfill. Materials Research Express. 2022;9.
39. John MJ, Thomas S. Biofibres and biocomposites. Carbohydrate Polymers. 2008;71(3):343-364.
40. Kabir MM, Wang H, Aravinthan T, Cardona F, Lau KT. Effects of natural fibre surface on composite properties: a review. Energy, Environment. Sustainability. eddBE Proceedings. 2011;94-99.
41. Karimi HR, Bidadi J, Aliha MRM, et al. An experimental study and theoretical evaluation on the effect of specimen geometry and loading configuration on

recorded fracture toughness of brittle construction materials. Journal of Building Engineering. 2023;75:106759.

42. Khalid MY, Al Rashid A, Arif ZU, Ahmed W, Arshad H, Zaidi AA. Natural fiber reinforced composites: sustainable materials for emerging applications. Results Engineering. 2021;11:100263.
43. Kou Y, Li G, Song Z, Wang P. Experimental study on the evolutive shear fracture behaviour and properties of cemented paste backfill. Construction and Building Materials. 2024;423:135780.
44. Kumar A, Walia BS, Mohan J. Compressive strength of fiber reinforced highly compressible clay. Construction and Building Materials. 2006;20(10):1063-1068.
45. Kuruppu MD, Chong KP. Fracture toughness testing of brittle materials using semi-circular bend (SCB) specimen. Engineering Fracture Mechanics. 2012;91:133-150.
46. Larsen IL, Thorstensen RT. The influence of steel fibres on compressive and tensile strength of ultra high performance concrete: a review. Construction and Building Materials. 2020;256:119459.
47. Cui L, Fall M. Mechanical and thermal properties of cemented tailings materials at early ages: Influence of initial temperature, curing stress and drainage conditions. Construction and Building Materials. 2016;125:553-563.
48. Latifi MR, Biricik Ö, Mardani A. Mechanical and durability performance of macro polypropylene fibrous concrete. Iranian Polymer Journal. 2023;32:1149–1164.
49. Lee J, Lopez MM. An experimental study on fracture energy of plain concrete. International Journal of Concrete Structures and Materials. 2014;8:129–139.

50. Li Z, Wang X, Wang L. Properties of hemp fibre reinforced concrete composites. Composites Part A: Applied Science and Manufacturing. 2006;37(3):497-505.
51. Li Z, Shi X, Chen X. Effect of rice straw on tensile properties of tailings cemented paste backfill. Applied Sciences. 2022;12:526.
52. Libos ILS, Cui L, Liu X. Effect of curing temperature on time-dependent shear behavior and properties of polypropylene fiber-reinforced cemented paste backfill. Construction and Building Materials. 2021;311:125302.
53. Libos I, Cui L. Mechanical properties and behavior of early-age fiber-reinforced cemented paste backfill. 2020.
54. Libre RGD Jr, Leaño JL Jr, Lopez LF, Cacanando CJD, Promentilla MAB, Ongpeng JMC. Microstructure and mechanical performance of bamboo fiber reinforced mill-scale—fly-ash based geopolymer mortars. Cleaner Chemical Engineering. 2023;6:100110.
55. Lilargem Rocha D, Tambara Júnior LUD, Marvila MT, et al. a review of the use of natural fibers in cement composites: concepts, applications and Brazilian history. Polymers (Basel). 2022;14(10):2043.
56. Liu S, Chao YJ, Zhu X. Tensile-shear transition in mixed mode I/III fracture. International Journal of Solids and Structures. 2004;41(22-23):6147-6172.
57. Lou J, Gao F, Yang J, et al. Characteristics of evolution of mining-induced stress field in the longwall panel: insights from physical modeling. International Journal of Coal Science & Technology. 2021;8:938–955.
58. Mitchell RJ, Stone DM. Stability of reinforced cemented backfills. Canadian Geotechnical Journal. 1987;24(2):189-197.

59. Mohanty AK, Misra M, Drzal LT. Sustainable bio-composites from renewable resources: opportunities and challenges in the green materials world. Journal of Polymers and the Environment. 2002;10:19–26.
60. Nasir O, Fall M. Shear behaviour of cemented pastefill-rock interfaces. Engineering Geology. 2008;101(3-4):146-153.
61. Özodabaş A. Reinforcement of cementitious mortars with hemp fibers and shives. Open Chemicals. 2023;21.
62. Pakravan HR, Latifi M, Jamshidi M. Hybrid short fiber reinforcement system in concrete: a review. Construction and Building Materials. 2017;142:280-294.
63. Pan AN, Grabinsky MWF, Guo L. Shear properties of cemented paste backfill under low confining stress. Advances in Civil Engineering. 2021;7561977:11.
64. Park SS. Unconfined compressive strength and ductility of fiber-reinforced cemented sand. Construction and Building Materials. 2011;25(2):1134-1138.
65. Pereira Prado L, Carrazedo R, El Debs MK. Interface strength of high-strength concrete to ultra-high-performance concrete. Engineering Structures. 2022;252:113591.
66. Pickering KL, Efendy MGA, Le TM. A review of recent developments in natural fibre composites and their mechanical performance. Composites Part A: Applied Science and Manufacturing. 2016;83:98-112.
67. Ponikiewski T, Katzer J, Bugdol M, Rudzki M. Determination of 3D porosity in steel fibre reinforced SCC beams using X-ray computed tomography. Construction and Building Materials. 2014;68:333-340.

68. Qiu X, Yang J, Wu Y, Yan L, Liu Q. Effect of fiber content on mechanical properties of fiber-reinforced CGF all-solid-waste binder-solidified soil. Materials. 2024;17(2):388.
69. Robert J. Mitchell and David M. Stone. 1987. Stability of reinforced cemented backfills. Canadian Geotechnical Journal. 24(2): 189-197.
70. Sanya OT, Shi J. Ultra-high-performance fiber reinforced concrete review: constituents, properties, and applications. Innovative Infrastructure Solutions. 2023;8:188.
71. Sharma P, Mali HS, Dixit A. Mechanical behavior and fracture toughness characterization of high strength fiber reinforced polymer textile composites. Iranian Polymer Journal. 2021;30:193–233.
72. Simões T, Costa H, Dias-da-Costa D, Júlio E. Influence of fibres on the mechanical behaviour of fibre reinforced concrete matrixes. Construction and Building Materials. 2017;137:548-556.
73. Suresh S, Tschegg EK. Combined mode I-mode III fracture of fatigue-precracked alumina. Journal of American Ceramic Society. 1987;70(10):726–733.
74. Summerscales J, Dissanayake NPJ, Virk AS, Hall W. Influence of polypropylene fiber geometry on plastic shrinkage cracking in concrete. Cement and Concrete Research. 2010;41(10):1329-1335.
75. Sun L, Fu J, Wang D, et al. Investigating the effect of various fibers on plasticity and compressive strength of concrete samples. Strength of Materials. 2024;56:200–208.

76. Tikou B, Benzaazoua M. An overview on the use of paste backfill technology as a ground support method in cut-and-fill mines. Proceedings of the Fifth International Symposium on Ground Support in Mining and Underground Construction. 2004:28-30.
77. Toledo Filho R, Joseph K, Ghavami K, England G. The use of sisal fibre as reinforcement in cement-based composites. Revista Brasileira de Engenharia Agrícola e Ambiental. 1999;3:245-256.
78. Väisänen T, Das O, Tomppo L. A review on new bio-based constituents for natural fiber-polymer composites. Journal of Cleaner Production. 2017;149:582-596.
79. Veigas MG, Najimi M, Shafei B. Cementitious composites made with natural fibers: Investigation of uncoated and coated sisal fibers. Case Studies in Construction Materials. 2022;16.
80. Visković J, Zheljazkov VD, Sikora V, et al. Industrial hemp (cannabis sativa L.) agronomy and utilization: a review. Agronomy. 2023;13(3):931.
81. Widodo E, Pratikto, Sugiarto, Widodo TD. Comprehensive investigation of raw and NaOH alkalized sansevieria fiber for enhancing composite reinforcement. Case Studies in Chemical and Environmental Engineering. 2024;9:100546.
82. Wu Z, Shi C, He W, Wu L. Effects of steel fiber content and shape on mechanical properties of ultra high-performance concrete. Construction and Building Materials. 2016;103:8-14.
83. Xie T, Ozbakkaloglu T. Behavior of steel fiber-reinforced high-strength concrete-filled FRP tube columns under axial compression. Engineering Structures. 2015;90:158-171.

84. Xiu Z, Wang S, Ji Y, Wang F, Ren F, Nguyen VT. Loading rate effect on the uniaxial compressive strength (UCS) behavior of cemented paste backfill (CPB). Construction and Building Materials. 2021;271:121526.
85. Xue G, Yilmaz E, Song W, Cao S. Fiber length effect on strength properties of polypropylene fiber reinforced cemented tailings backfill specimens with different sizes. Construction and Building Materials. 2020;241:118113.
86. Xue G, Yilmaz E, Song W, Yilmaz E. Influence of fiber reinforcement on mechanical behavior and microstructural properties of cemented tailings backfill. Construction and Building Materials. 2019;213:275-285.
87. Yan L, Kasal B, Huang L. A review of recent research on the use of cellulosic fibres, their fibre fabric reinforced cementitious, geo-polymer and polymer composites in civil engineering. Composites Part B: Engineering. 2016;92:94-132.
88. Yilmaz E. Stope depth effect on field behaviour and performance of cemented paste backfills. International Journal of Mining, Reclamation and Environment. 2017;32(4):273–296.
89. Yilmaz E, Belem T, Bussière B, Benzaazoua M. Relationships between microstructural properties and compressive strength of consolidated and unconsolidated cemented paste backfills. Cement and Concrete Composites. 2011;33(6):702-715.
90. Yin S, Hou Y, Chen X, Zhang M. Mechanical, flowing and microstructural properties of cemented sulfur tailings backfill: effects of fiber lengths and dosage. Construction and Building Materials. 2021;309:125058.

91. Yu Z, Wang Y, Li J. Performance investigation and cost–benefit analysis of recycled tire polymer fiber-reinforced cemented paste backfill. Polymers. 2022;14(4):708.
92. Zhang C, Sun Y, Xu J, Wang B. The effect of vibration mixing on the mechanical properties of steel fiber concrete with different mix ratios. Materials. 2021;14:3669.
93. Zhao Z, Cao S, Yilmaz E. Polypropylene fiber effect on flexural strength, toughness, deflection, failure mode and microanalysis of cementitious backfills under three-point bending conditions. Minerals. 2023;13(9):1135.
94. Zhou N, Du E, Zhang J, Zhu C, Zhou H. Mechanical properties improvement of sand-based cemented backfill body by adding glass fibers of different lengths and ratios. Construction and Building Materials. 2021;280:122408.
95. Zhou X, Saini H, Kastiukas G. Engineering properties of treated natural hemp fiber-reinforced concrete. Frontiers in Built Environment. 2017;3.
96. Zhu C, Zhang J, Nan Z, Li M, He Z. Effects of doping glass fibers on the early strength of sand-based cemented paste backfill for solid wastes disposal in a coal mine. Advances in Civil Engineering. 2021;2021(1):5554941.
97. Zhu C, Zhou N, Guo Y, Li M, Cheng Q. Effect of doped glass fibers on tensile and shear strengths and microstructure of the modified shotcrete material: an experimental study and a simplified 2D model. Minerals. 2021;11(10):1053.
98. Zhanguo X, Fanzhen M, Feili W, Shuhong W, Yingchun J, Qinkuan H. Shear behavior and damage evolution of the interface between rough rock and cemented tailings backfill. Theoretical and Applied Fracture Mechanics. 2023;125:103887.

99. Zihai Shi. Crack Analysis in Structural Concrete: Theory and Applications. Butterworth-Heinemann, an imprint of Elsevier; 2009.